Paleoceanography and Paleoclimatology

RESEARCH ARTICLE
10.1029/2025PA005141

Seasonal Changes in Marine Archaeal Tetraether Lipid Export Depth Linked to Net Primary Productivity

Addison Rice[1,2], Eunmi Park[3,4,5], Gesine Mollenhauer[3,4,5], Daisy Bouwmans[1], Anouk van Boxtel[1,6], Gert J. de Lange[1], Ryan Paul[1], Francesca Sangiorgi[1], Ryan Smulders[1], Jan-Berend Stuut[6,7], Martin Ziegler[1], Appy Sluijs[1], and Francien Peterse[1]

[1]Department of Earth Sciences, Utrecht University, Utrecht, The Netherlands, [2]Now at Department of Earth Sciences, ETH Zürich, Zürich, Switzerland, [3]Alfred Wegener Institute, Helmholtz Center for Polar and Marine Research, Bremerhaven, Germany, [4]MARUM Centre for Marine Environmental Sciences, University of Bremen, Bremen, Germany, [5]Department of Geosciences, University of Bremen, Bremen, Germany, [6]Department of Ocean Systems, NIOZ, Texel, The Netherlands, [7]Department of Earth Sciences, Vrije Universiteit Amsterdam, Amsterdam, The Netherlands

Abstract Marine ammonia oxidizing archaea (AOA) produce isoprenoid glycerol dibiphytanyl glycerol tetraethers (GDGTs) which form the basis of seawater temperature proxy TEX_{86}. Although most studies use TEX_{86} for sea surface temperature (SST) reconstructions, maximum GDGT production occurs at and below the nitracline. Moreover, sedimentary GDGT-2/GDGT-3 values >5 reflect GDGT contributions of a deeper dwelling (>100 m) clade of AOA, fueling debate on export mechanisms and the water depth of TEX_{86} proxy sensitivity. We investigate subseasonal variations in GDGT export depth using 4 new and 19 previously published marine sediment trap records and compare results to real-time biogeochemical and physical hindcast/reanalysis model outputs. Due to the complexity of the biological pump and the often short time series of sediment trap records, no globally consistent pattern emerges. However, GDGT-2/GDGT-3 ratios imply seasonal changes in GDGT export depth, and often correlate to changes in the depth (negative) or intensity (positive) of maximum net primary production (NPP). Increased/shallower maximum NPP also correlate positively with GDGT flux at several sites, indicating that NPP exerts a strong control on GDGT origin depth. Mechanistically, increased/shallower maximum NPP incorporates relatively more shallow clade GDGTs into sinking particles, leading to lower GDGT-2/GDGT-3 values. Additionally, GDGT-2/GDGT-3 values correlate with TEX_{86} in most sediment traps, suggesting that, on sub-annual timescales, mixing of shallow and deep-clade derived GDGTs rather than SST changes causes variations in TEX_{86}. TEX_{86}-based temperatures are up to 0.5°C lower per unit increase in GDGT-2/GDGT-3, but the North Atlantic deviates from this global trend with a positive correlation.

Plain Language Summary Variations in the number of rings in archaeal tetraether membrane lipids present in marine sediments are at the base of a widely used marine paleothermometer. Although this temperature proxy correlates well with sea surface temperature in modern sediments, the lipids are mostly produced deeper in the water column (>50 m). In addition, two depth-differentiated groups of archaea produce these lipids. The lipids produced by deeper dwelling (>100 m) archaea do not relate to temperature but can influence the proxy. Therefore, the water column depth at which sedimentary lipids were originally produced, and thus the temperature signal they preserve, is unclear. We here show that the origin depth of the lipids captured in a global set of sediment traps catching sinking particles often relates to net primary production. This suggests that changes in the depth and amount of phytoplankton production influence lipid distributions, in addition to temperature. For paleoclimate studies, this means that productivity-related variations in the origin depth of these lipids through time should be considered when interpreting reconstructions from ancient sediments in a paleotemperature context.

Key Points:

- Global marine sediment traps record seasonal changes in archeal tetraether lipid export from two depth-differentiated ecological groups
- Contribution of shallow-clade archaeal tetraethers increases with net primary production, suggesting a productivity control on export
- Larger relative proportions of deep clade archaeal tetraethers can lead to offset proxy temperatures in sinking particles

Supporting Information:

Supporting Information may be found in the online version of this article.

Correspondence to:

A. Rice,
adrice@ethz.ch

Citation:

Rice, A., Park, E., Mollenhauer, G., Bouwmans, D., van Boxtel, A., de Lange, G. J., et al. (2026). Seasonal changes in marine archaeal tetraether lipid export depth linked to net primary productivity. *Paleoceanography and Paleoclimatology*, *41*, e2025PA005141. https://doi.org/10.1029/2025PA005141

Received 18 FEB 2025
Accepted 23 JAN 2026

1. Introduction

Ammonia oxidizing archaea (AOA) of the order Nitrososphaerales (formerly Thaumarchaeota and Crenarchaeota) are ubiquitous in Earth's oceans, accounting for ~20% of the prokaryotic cells in the water column (Karner et al., 2001; Könneke et al., 2005; Wuchter, Abbas, et al., 2006). Marine Nitrososphaerales produce isoprenoid glycerol dibiphytanyl glycerol tetraethers (isoGDGTs), a suite of recalcitrant membrane-spanning lipids (Wuchter et al., 2004). These molecules contain 0-4 cyclopentane moieties (referred to as GDGT-n,

where n is the number of cyclopentane moieties), or one cyclohexane and four cyclopentane moieties (cren-archaeol (cren) and its isomer (cren')). GDGT-0, -1, -2, -3, cren and cren' are commonly detected in marine sediments (De Rosa & Gambacorta, 1988; Schouten et al., 2000). Globally, the number of rings incorporated in GDGTs measured in marine surface sediments correlates to sea surface temperature (SST) (Schouten et al., 2002). This led to the development and use of a GDGT distribution-based SST proxy termed TEX_{86}, which is defined as:

$$TEX_{86} = \frac{GDGT-2 + GDGT-3 + Cren'}{GDGT-1 + GDGT-2 + GDGT-3 + Cren'} \quad (1)$$

(Schouten et al., 2002). Mesocosm and culture studies have confirmed that *Nitrososphaera* adapt the molecular composition of their membranes to temperature, where GDGTs with more rings form at higher temperatures, although different strains vary in the exact adjustment of GDGT distributions to changes in growth temperature (Elling et al., 2015; Wuchter et al., 2004). Despite use as an SST proxy, maximum GDGT production is not necessarily in the photic zone, but slightly deeper in the water column, near the nitracline (typically ~40–250 m depth), reflecting the ammonia oxidizing role of *Nitrososphaera* (Hernández-Sánchez et al., 2014; Hurley et al., 2018; Sinninghe Damsté et al., 2002; Turich et al., 2007). Moreover, TEX_{86} values in marine surface sediments correlate not only to SST, but also to shallow subsurface (100 m depth) temperature (Schouten et al., 2002). Although this has been attributed to the close correlation between shallow subsurface temperatures and SSTs (Schouten et al., 2002), the origin depth of sedimentary GDGTs and, therefore, the exact temperature signal they reflect remains a subject of extensive debate (Ho & Laepple, 2016; Hurley et al., 2018; Schouten et al., 2002; Taylor et al., 2013; Tierney & Tingley, 2014; van der Weijst et al., 2022). As a result, the currently most frequently applied calibrations in paleotemperature studies relate TEX_{86} to both SST (mixed layer) and integrated 0–200 m temperatures (Kim et al., 2008, 2010; Tierney & Tingley, 2014, 2015). Other studies suggest a deeper GDGT origin depth because of the scarcity of isoGDGT production in the mixed layer (Hurley et al., 2018; Sinninghe Damsté et al., 2002), and calibrate TEX_{86} to for example, 100–250 (Fokkema et al., 2023) or 100–350 m (van der Weijst et al., 2022) for a conservative endmember.

In addition, *Nitrososphaera* can be divided into two clades, one of which inhabits the uppermost water column (shallow clade, ~0–200 m) while the other resides in deeper waters (deep clade, >100 m), with overlapping habitat depth (Besseling et al., 2019; Francis et al., 2005; Villanueva et al., 2015). Shallow and deep waters contain GDGTs in distinct distributions, which is most pronounced in the ratio between GDGT-2 and GDGT-3 (Besseling et al., 2019; Hernández-Sánchez et al., 2014; Rattanasriampaipong et al., 2022; Taylor et al., 2013). In a study quantifying both genetic material and GDGT distributions in the water column, the change in dominant AOA clade coincides with changes in GDGT-2/GDGT-3 (Besseling et al., 2019). Water profile studies examining GDGTs in suspended matter indicate that this ratio increases with water depth, reflecting an increasingly higher contribution of GDGTs produced by the deep clade (e.g., Hernández-Sánchez et al., 2014; Hurley et al., 2018; Kim et al., 2015). The presence of GDGT-2/GDGT-3 ratio values >5 in surface sediments, which is especially common in sediments >1,000 m water depth, is considered an indication that GDGTs from the deep clade substantially contribute to the total GDGT pool stored in sediments (Taylor et al., 2013). Furthermore, compound-specific radiocarbon measurements have shown that sedimentary GDGTs originate, at least in part, in subsurface waters (Shah et al., 2008). While the shallow clade appears to adjust the distribution of GDGTs in their cell membranes in response to temperature, core lipid GDGTs from below 100 m water depth do not show this temperature relationship (Hernández-Sánchez et al., 2014; Hurley et al., 2018; Schouten et al., 2002; Taylor et al., 2013; Turich et al., 2007; Wuchter et al., 2005; Zhu et al., 2016). Although TEX_{86} values in SPM >100 m depth can be similar to those near the sea surface, suggesting little influence of deep clade archaea on TEX_{86} values (e.g., Hernández-Sánchez et al., 2014; Schouten et al., 2002), GDGTs from deep clade archaea have been shown to greatly influence sedimentary TEX_{86} values in the Mediterranean Sea (Besseling et al., 2019; Kim et al., 2015). Consequently, (large) contributions of deeper clade GDGTs may therefore alter the temperature signal of shallow clade-GDGTs preserved in marine sediments.

Importantly, a mechanism which allows for large proportions of GDGT export from the deep clade remains unclear. Archeal cells are small and neutrally buoyant and require packaging into larger particles to sink. Although some fecal pelleting occurs in the ocean's twilight zone, most sinking particulate organic matter originates in the euphotic zone (typically <100 m) in the form of phytoplankton remains, marine snow aggregates, and fecal pellets (Turner, 2002). Remains of picophytoplankton in the same size range as AOA (0.2–2 μm) can be

exported through these mechanisms, and can comprise a large proportion of organic matter export (Close et al., 2013; Richardson, 2019; Richardson & Jackson, 2007). In fact, studies on GDGTs in sediment trap material note relationships between GDGT flux and remains of primary producers as indicated by phytol (Wuchter, Schouten, et al., 2006), carbonate (Chen et al., 2016; Mollenhauer et al., 2015; Park et al., 2019; Yamamoto et al., 2012), and opal (Chen et al., 2016; Mollenhauer et al., 2015; Park et al., 2018, 2019), suggesting that the majority of the GDGTs are packaged in the euphotic zone prior to export. However, particle (re-)packaging at depths below 100 m could lead to enhanced export of deep clade-derived GDGTs. Despite the limited understanding of GDGT export mechanisms, notably the most important factor determining export depth, a systematic, large-scale study on GDGT export is still lacking.

We hypothesize that the biological pump controls GDGT export dynamics, and specifically that the GDGT export production depth and the quantity of GDGTs exported is related to the depth and quantity of net primary production (NPP). Because NPP quantifies the export of primary producers in the upper ocean, it may also reflect the proportion of GDGTs from shallow clade archaea incorporated into sinking particles. To test this hypothesis, we compiled GDGT data from 4 new and 19 previously published globally distributed sediment trap sites (Table 1; Figure 1). Multiple (2–10) years of data are available for 7 sites, allowing for robust statistical assessment of seasonal variability. In addition, sediment traps were moored at multiple depths at 11 sites (3 of which are also multi-year sites), allowing for comparison between trap depths as particles sink through the water column. We use the GDGT-2/GDGT-3 ratio as an indicator of changing GDGT export production depth (hereafter origin depth) and compare it with real-time model-based NPP and nitrate concentrations. Doing so allows us to test whether, on seasonal time scales, GDGT origin depth reflects the depth of GDGT production, as indicated by the depth of the nitracline or the nitrate concentration at the nitracline, or the depth of particle aggregation, as indicated by the amount and depth of maximum NPP. Subsequently, we examine spatial patterns in the correlations between TEX_{86} and GDGT-2/GDGT-3 in sinking and suspended particles to understand to what extent and under which conditions contributions of GDGTs from the deep clade might impact TEX_{86}-based temperatures in sediment.

2. Materials and Methods

2.1. Site Selection and GDGT Analysis

We analyzed the distribution and absolute abundances of GDGTs in settling particles collected by sediment traps moored in the eastern Mediterranean Sea, under seasonal sea ice in the Ross Sea, and at two locations with differing trophic states in the western tropical South Atlantic. We further compiled previously published GDGT distributions in sinking particles at 19 sites across the globe (Figure 1, Table 1).

Full details on depths, timings, buffering, and poisoning of the newly reported sediment trap samples are presented in Table S1 in Supporting Information S1.

2.1.1. Eastern Mediterranean Sea

Sediment traps were moored in the eastern Mediterranean Sea at Bannock Basin (34.37°N, 20.04°E) at three water depths in the oxic portion of the water column (~800, 2,000, and 3,000 m; Table S1 in Supporting Information S1) between 1999 and 2011 and at the MedDust site (34.97°N, 18.03°E) at 2,340 m between 2017 and 2018. Collected material was split eight ways after recovery, where two splits on glass fiber filters were used for lipid extraction. Material collected at the MedDust site was split five ways, where one split was used for lipid extraction. The sediment trap material as well as surface sediment (0–0.5 cm) from box core SL139BC5 (34.27°N, 19.83°E) was freeze-dried and extracted in DCM:methanol 9:1 using a microwave extraction system. The resulting Total Lipid Extracts (TLEs) were passed over a Na_2SO_4 column with DCM:methanol 9:1. Most TLEs (aside from NU series samples, June 2004 to September 2005) then underwent acid hydrolysis and methylation. Acid hydrolysis was performed using 2M HCl in methanol for 2 hours at 70°C. After cooling, 1 mL MilliQ was added. Hydrolyzed TLEs were extracted three times with DCM, dried, and passed over a second Na_2SO_4 column with DCM:methanol 9:1. Hydrolyzed TLEs were then methylated in DCM:methanol 1:1 with 10 µL 0.2 M trimethylsilyldiazomethane for 30 min. The methylated TLEs were dried, dissolved in ethyl acetate, and eluted over a column of non-activated silica gel topped with Na_2CO_3. Finally, methylated TLEs were separated into three fractions with increasing polarity (apolar, ketone, and polar) using an aluminum oxide column and hexane:DCM (9:1), hexane:DCM (1:1), and DCM:methanol (1:1), respectively. A known amount of C_{46} GTGT standard was added to the polar fraction for quantification of GDGTs. The polar fraction was dissolved in hexane:isopropanol (99:1) and filtered using a

Table 1
Overview of New and Reviewed Sediment Trap Locations

Site ID	Site name (this study)	Mooring name	Latitude	Longitude	Depth	Date start	Date end	Sample count[a]	Source
APF	Antarctic Polar Front	PF3	−50.13	5.83	614; 3,196	1989-11-10	1990-12-23	17, 8	Park et al. (2019)
AS	Arabian Sea	MS-3	17.2	59.6	500; 1,500; 3,000	1994-11-11	1995-12-24	13, 13, 15	Wuchter, Schouten, et al. (2006)
BS[b]	Baltic Sea	-	57.305	19.88	198	2010-05-01	2011-01-31	17	Wittenborn et al. (2022)
CB	Cape Blanc	CBeu	20.75	−18.7	1,296	2003-07-15	2007-03-23	71	Mollenhauer et al. (2015)
CrB[b]	Cariaco Basin	Trap A/ Trap B	10.5	−64.67	275; 930	1999-05-01	2003-07-01	49, 53	Turich et al. (2013)
CTNA	central tropical North Atlantic	M2	13.81	−37.82	1,235; 3,490	2012-10-19	2013-11-07	24, 24	de Bar et al. (2019)
EMS	Eastern Mediterranean	BB	34.37	20.04	~800; 2,000; 3,000	1999-09-15	2011-04-21	132, 197, 196	This study
EMS	Eastern Mediterranean	MedDust	34.96	18.03	2,340	2017-04-14	2018-05-19	40	This study
ETNA	eastern tropical North Atlantic	M1	12	−23	1,150	2012-10-19	2013-11-07	24	de Bar et al. (2019)
FS	Fram Strait	FEVI16	79.02	4.35	1,296	2007-07-23	2008-06-30	16	Park et al. (2019)
GB	Guinea Basin	GBN3	1.8	−11.13	853; 3,921	1989-03-01	1990-03-16	20, 19	Park et al. (2018)
GoC	Gulf of California	-	27.88	−111.67	500	1996-02-11	1997-01-19	11	McClymont et al. (2012)
GoM	Gulf of Mexico	-	27.5	−90.3	700	2010-01-10	2013-12-09	105	Richey and Tierney (2016)
MC	Mozambique Channel	-	−16.8	40.8	2,250	2003-11-23	2009-01-04	58	Fallet et al. (2011)
NC	Namibian Coast	LZ	−25.28	13.05	960	2000-02-17	2001-01-28	18	Park et al. (2018)
NEA	northeast Atlantic	L2	47.833	−19.65	3,500	1992-05-06	1992-11-25	10	Auderset et al. (2019)
NWP	northwest Pacific	WCT-2	39	147	1,350; 2,800; 4,750	1997-11-19	1999-08-10	38, 24, 36	Yamamoto et al. (2012)
RS[b]	Ross Sea	Mooring A	−76.68	169.02	392; 789	2008-02-01	2009-02-01	9, 9	This study
SBB	Santa Barbara Basin	–	34.23	−120.03	490	1995-12-30	1997-12-25	23	Huguet et al. (2007)
SNA	subpolar North Atlantic	St1	62.00	−16.00	1,850	2011-07-15	2012-07-15	21	Rodrigo-Gamiz et al. (2015)
SoJ	South of Java	JAM2	−8.29	108.03	2,200	2001-12-14	2002-11-15	20	Chen et al. (2016)
WTNA	western tropical North Atlantic	M4	12.06	−49.19	1,130; 3,370	2012-10-19	2013-11-07	24, 23	de Bar et al. (2019)
WTSA1	western tropical South Atlantic 1	WA9	−7.5	−28.1	591; 4,456	1996-03-23	1997-02-26	13, 16	This study
WTSA2	western tropical South Atlantic 2	WAB1	−11.53	−28.52	727; 4,515	1997-02-27	1998-05-19	16, 9	This study

[a]Count of samples with all GDGTs above the detection limit. Where multiple numbers are present, these correspond to different trap depths. [b]All GDGT-2/GDGT-3 values <5.

0.45 µm PTFE filter prior to HPLC-MS analysis, which was performed using an Agilent 1260 Infinity ultra-high-performance liquid chromatographer coupled to an Agilent 6130 single quadrupole mass detector according to the method of Hopmans et al. (2016). Chromatograms resulting from selected ion monitoring of m/z 744, 1,302, 1,300, 1,298, 1,296, and 1,292 were used to quantify the GDGT standard, GDGT-0, GDGT-1, GDGT-2, GDGT-3, and crenarchaeol and cren', respectively.

2.1.2. Ross Sea

Mooring A was deployed in the southernmost part of the Joides Basin (76.68°S, 169.02°E, water depth ~800 m) with sediment traps at 392 and 789 m in the water column. Sinking particulate matter collected by the trap was centrifuged and decanted, where decanted fluid was passed over a glass fiber filter to ensure no loss of material. Both filters and centrifuged sample pellets were freeze-dried and pellets were crushed prior to 40-hr Soxhlet

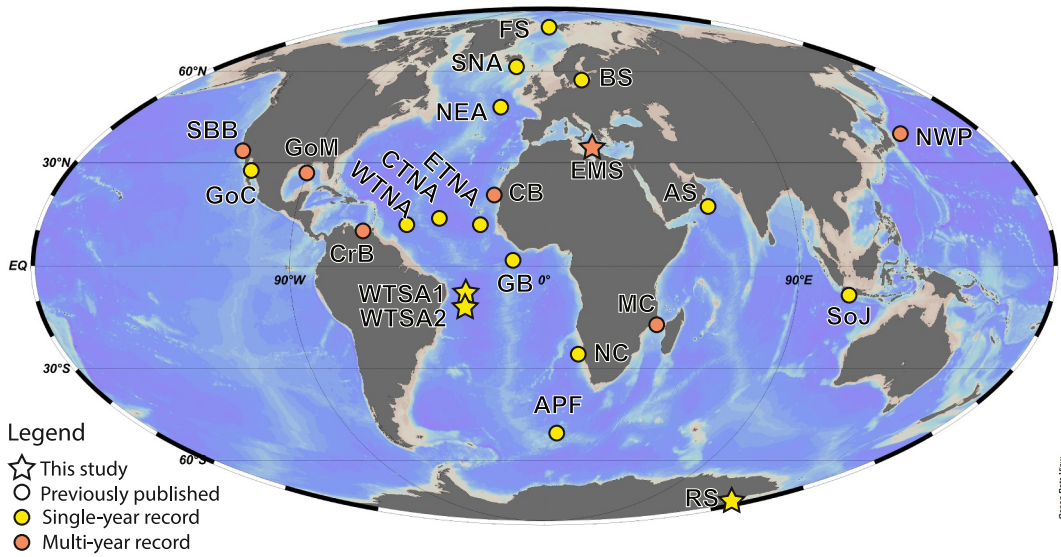

Figure 1. Sediment trap locations with abbreviations used in this study as in Table 1 (Auderset et al., 2019; Chen et al., 2016; de Bar et al., 2019; Fallet et al., 2011; Huguet et al., 2007; McClymont et al., 2012; Mollenhauer et al., 2015; Park et al., 2018, 2019; Richey & Tierney, 2016; Rodrigo-Gámiz et al., 2015; Turich et al., 2013; Wuchter, Schouten, et al., 2006; Yamamoto et al., 2012).

extraction with DCM:MeOH 7.5:1. An 80% aliquot of the lipid extract was used to for further analysis and separated into apolar and polar fractions using an aluminum oxide column and hexane:DCM (9:1) and DCM: methanol (1:1) for the two fractions, respectively. An internal C_{46} GTGT standard was added to the polar fraction for quantification. The resulting residue was dissolved in hexane:isopropanol (99:1) and injected into an Agilent 1100 series LC coupled to a HP 1100 APCI-MS according to Schouten et al. (2007) with minor modifications. GDGT abundances were quantified as above.

2.1.3. Western Tropical South Atlantic

Two moorings (WTSA1 and WTSA2) were deployed in the central Brazil Basin, equipped with Kiel-type 0.5 m^2 sediment traps. Sediment trap material was split into 5 parts, and 5–160 mg of this material, as well as surface sediment (GeoB 5,201-8; 28.5°W, 11.5°S) collected at the WTSA2 trap location was selected for lipid analysis. An internal C_{46} GTGT standard was added to each sample prior to ultrasonic extraction (3x) with DCM:MeOH (9:1). The resulting extracts were saponified with 1 mL 0.1 M KOH in methanol:water (9:1) at 80°C for 2 hours. Neutral lipids were recovered in hexane and then separated into apolar, ketone, and polar fractions using a deactivated silica gel (1% wt) column and eluting with 2 mL hexane, 4 mL hexane:DCM (2:1), and 4 mL DCM: methanol (9:1), respectively. The polar fraction was dissolved in hexane:isopropanol (99:1) and filtered using a 0.45 μm PTFE filter prior to GDGT analysis using an Agilent 1200 Series high performance liquid chromatography system with an Agilent 6210 quadrupole mass spectrometer using atmospheric pressure chemical ionization, following the method of Schouten et al. (2007). GDGTs were quantified as detailed above.

2.1.4. Data Comparison Across Analytical Methodologies

The compilation presented here contains GDGT distributions produced through several different extraction, workup, and analytical procedures. Based on interlaboratory comparison studies, differences in extraction methods do not significantly impact GDGT distributions (De Jonge et al., 2024; Schouten et al., 2013). However, harsh extraction techniques, or gentle extraction techniques combined with the use of acid or base hydrolysis could impact GDGT distributions by resulting in measurement of a mixture of core lipid and intact polar lipid (IPL) GDGTs (Text S1 in Supporting Information S1; Huguet et al., 2010; Lengger et al., 2012). The possible impact of acid hydrolysis on GDGT distributions was evaluated for the eastern Mediterranean Sea sediment trap, but this did not reveal substantial offsets (Figure S1 in Supporting Information S1). Furthermore, differences in

GDGT distributions between sites do not show a consistent pattern that can be related to differences in methodology. The methodology used at each site is compiled in Table S2 of Supporting Information S1.

Notably, differences in analytical methodology can affect GDGT quantification. For example, the Arabian Sea data set was produced using the total ion chromatograms, rather than extracted ion chromatograms, leading to greater uncertainty in the GDGT quantification at this site. Furthermore, interlaboratory comparison studies have shown that quantification of GDGTs in the same sample material can differ by over three orders of magnitude between laboratories (De Jonge et al., 2024; Schouten et al., 2013). Among the 18 sites included in this study for which GDGTs are quantified, the GDGT flux varies by seven orders of magnitude (Table S3 in Supporting Information S1). Given that the maximum range of variation in the 10-year timeseries for the Eastern Mediterranean Sea is four orders of magnitude, we refrain from directly comparing fluxes between sites. Instead, we focus on comparing the timing and relative amplitude of GDGT fluxes at each site. During data compilation, units of the reported GDGT distributions were retained, except where raw integrated peak areas were provided, which were converted to flux where sufficient information allowed for quantification, or else to fractional abundances of the six isoprenoid GDGTs. For quality control, GDGT distributions which were considered unreliable following community agreement guidelines (Bijl et al., 2025) were flagged. Information on the reliability and inclusion of the GDGT data in the further analysis and plots is given in Table S3 of Supporting Information S1.

2.2. Nutrient Concentrations and NPP Time Series

Although depth habitat of ammonia oxidizing archaea would ideally be compared with ammonia concentrations, globally consistent hindcast data for ammonia are not available. Therefore, nitrate concentrations are used to track the depth of the nitracline and to indicate the depth of greatest GDGT production. In addition, NPP and the depth of maximum NPP, which indicate the depth of particle packaging, are used to describe the strength of the biological pump.

Nitrate concentrations and NPP in the 0–500 m water column of each sediment trap site were obtained from a biogeochemical hindcast model with daily, 0.25° resolution (E.U. Copernicus Marine Service Information (CMEMS), n.d.-a). The depth of the nitracline was determined as the depth interval with the greatest change in nitrate concentration per meter. The depth of the nitracline and the nitrate concentration at the nitracline were used to indicate changes in the nitracline. The depth of maximum NPP and the quantity of NPP at this depth were used to indicate changes in NPP. A physical reanalysis model (E.U. Copernicus Marine Service Information (CMEMS), n.d.-b) was used to obtain in situ temperatures at depths of 0, 25, 56, 78, and 110 m, with daily, 0.25° resolution. For correlation between model data and data derived from sediment traps, the modeled variables were averaged over the bottle open time assuming no time lag due to the fast sinking speed (>200 m/d) of most particulate organic matter (Wakeham et al., 2009). Pearson correlation coefficients were calculated and reported where they are significant at the 95% confidence level.

Real-time model data were available for all but three sediment traps (Antarctic Polar Front, Guinea Basin, Northeast Atlantic), which were operating prior to the 1993 start date of model data availability. Model data was only available for part of the year at two high-latitude sites (Fram Strait, Ross Sea) which were, therefore, excluded from comparison with model data. Furthermore, sites in which measured GDGT-2/GDGT-3 values were always <5 (Baltic Sea, Cariaco Basin, Ross Sea) were excluded in the assessment of factors that drive seasonal changes in shallow versus deep clade export.

3. Results

A large number of statistical tests ($n = 749$; Table S4 in Supporting Information S1) were performed, which could lead to numerous significant but spurious correlations. To avoid false positives and to obtain an overall 95% confidence, correlations are only presented here when present and in the same direction (either positive or negative) at a minimum of three sites with 95% significance. Due to the nature of statistical tests, the data-rich multi-year sites (7/23 sites) are more likely to yield significant correlations. As a result, significant findings often occur at relatively few sites (Table S4 in Supporting Information S1), but may nonetheless be globally important.

3.1. Patterns in GDGT Distributions and Fluxes in Sediment Traps

GDGT-2/GDGT-3 ratio values vary seasonally in 20 out of 23 sediment trap series (Figure 2ab; Figure S2 in Supporting Information S1). The seasonal variability in GDGT-2/GDGT-3 ratio values is largest in the eastern Mediterranean Sea, Cape Blanc, and the Gulf of Mexico, where the typical seasonal ranges are 10–18, 6–12, and 4–12, respectively. Notably, the use of the GDGT-2/GDGT-3 ratio can complicate the intuitive interpretation of ratio values. When considering this ratio as an indicator of end-member mixing, this ratio diminishes changes in GDGT distributions at lower (<5) ratio values and exaggerates changes in GDGT distributions at higher (>10) ratio values. A form of this ratio that yields a linear mixing line, that is, GDGT-2/(GDGT-2+GDGT-3) would resolve this issue. Although the GDGT-2/GDGT-3 ratio is used here to facilitate comparison with the literature, GDGT-2/(GDGT-2+GDGT-3) values for each site are shown on in Figure S2 in Supporting Information S1. In addition, the timing of high and low GDGT-2/GDGT-3 is not consistent across sites: low GDGT-2/GDGT-3 values occur in boreal/austral winter, spring, and summer without a clear spatial trend. TEX_{86} values in sinking particles at a given site typically vary seasonally by either >0.1 units (i.e., Arabian Sea, Cape Blanc, northwest Pacific) or <0.05 units (Figure 2c). Significant correlations between GDGT-2/GDGT-3 and TEX_{86} occur at 11 out of 20 sediment trap sites, although these correlations are positive at 6 sites and negative at 5 sites (Figure 3; Table S4 in Supporting Information S1). There also is a negative correlation between the GDGT flux and GDGT-2/GDGT-3 values at 8 out of 17 total sites (Figure 3; Table S4 in Supporting Information S1). Correspondingly, flux-weighted GDGT-2/GDGT-3 values are lower than sample-averaged GDGT-2/GDGT-3 values at these locations (Table S5 in Supporting Information S1). Notably, at the 11 sites with sediment traps moored at multiple depths, the flux-weighted (10/11 sites) and sample-averaged (9/11 sites) GDGT-2/GDGT-3 values show little change (<1.5) with depth (Table S5 in Supporting Information S1). However, the comparison between surface sediments and flux-weighted averages of sediment trap material yields mixed results; At 4/9 locations for which surface sediment data is available GDGT-2/GDGT-3 values in surface sediments are similar (<0.5 ratio values different) to flux-weighted average values in the sediment trap. At another 4/9 locations, GDGT-2/GDGT-3 values in sediments are 1.1–2.6 ratio values lower than sinking flux in the sediment trap, and at the remaining site (eastern tropical North Atlantic), the surface sediment GDGT-2/GDGT-3 value is 11 ratio values lower than the flux-weighted average in the sediment trap (Table S5 in Supporting Information S1). TEX_{86} values can also differ between sediments and flux-weighted average sediment trap values (Table S5 in Supporting Information S1). At 4/9 locations TEX_{86} values are >0.01 units higher in sediments than the flux-weighted average value in the overlying sediment trap. At 4 sites the sedimentary value differs ≤0.01 units, and at the remaining site (eastern tropical North Atlantic) the sedimentary TEX_{86} value is 0.04 units lower than the flux-weighted average in the sediment trap.

At eight sites GDGT flux data were available for multiple depths (Table S6 in Supporting Information S1). At six of these sites, the GDGT flux increases with depth. At 4/6 sites which show an increase in GDGT flux with depth, total mass flux also increases with depth.

3.2. Comparison of GDGT Distributions and Fluxes With Hindcast Model Outputs

Hindcast model output was compared with GDGT distributions at 16 sites for which hindcast model data was available for the full time series and GDGT-2/GDGT-3 values were above 5 at some time of year; and with GDGT fluxes at 13 sites for which GDGT flux was also quantified (Figure 3; Table S4 in Supporting Information S1). Notably, the data from the biogeochemical hindcast model can result in spurious correlations, for example, when cyclic changes in environmental variables are not truly independent of one another. Depending on the timing of their cyclicity, they may be closely related or out of phase, which can result in non-causative correlation when comparing these parameters with seasonal patterns in the GDGT data. Specifically, NPP and nitracline variables exhibit both positive and negative correlations with one another (Figure 3; Table S4 in Supporting Information S1), suggesting that some correlations between GDGT distributions and environmental variables may be incidental, rather than causative. Therefore, we here aggregate results from several sites to identify the causative variable explaining variations in GDGT distributions and fluxes. Importantly, modeled nitracline depth and nitrate concentration at the nitracline are closely positively correlated, so we do not consider these variables to be independent. Similarly, the depth of the NPP maximum and the maximum NPP are negatively correlated and not independent (Figure 3; Table S4 in Supporting Information S1). As a result, we do not discuss the depth and concentration variables separately, but consider significant results when they occur in either variable at a given site.

10.1029/2025PA005141

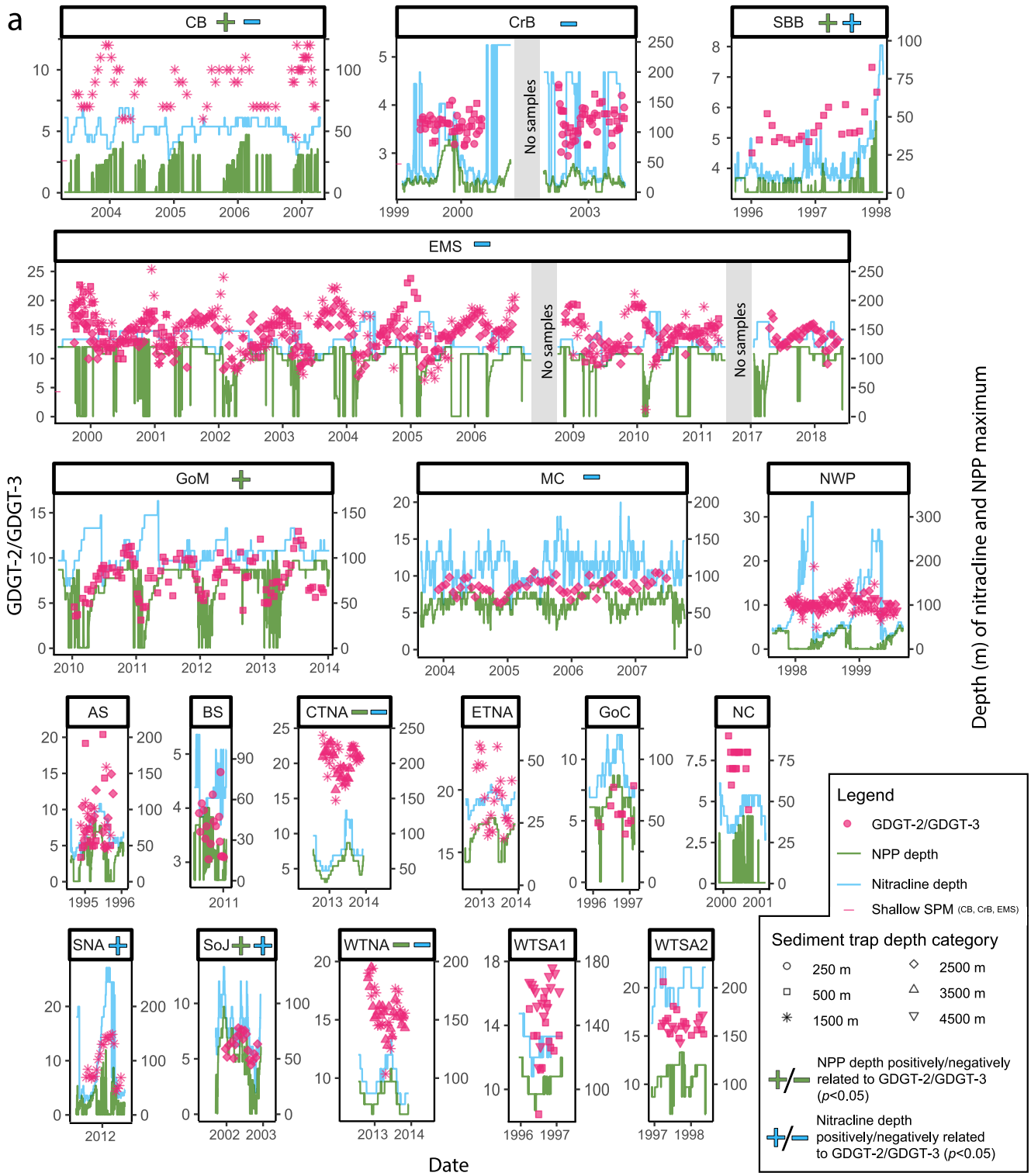

Figure 2. Time series of GDGT indices and modeled variables at global sediment trap sites, with site abbreviations as in Table 1 (a) GDGT-2/GDGT-3 (left axis) and depths of the nitracline and maximum NPP (right axis); (b) GDGT-2/GDGT-3 (left axis) and nitrate concentration at the nitracline and NPP concentration (right axis); and (c) model- and TEX_{86}-based temperatures (left axis; Kim et al., 2008) and TEX_{86} values (right axis). Note that the time axes for multi-year sites (CB, CrB, EMS, GoM, MC, NWP, and SBB) are exaggerated by 75% relative to single-year sites. Ticks on the date axis mark the first day of the year. Significant correlations are noted when present for any sediment trap depth at that location. Minimum GDGT-2/GDGT-3 values in shallow (<100 m) SPM are shown in (a) and (b) for sites CB (Basse et al., 2014), CrB (Wakeham et al., 2004), and EMS (Besseling et al., 2019).

10.1029/2025PA005141

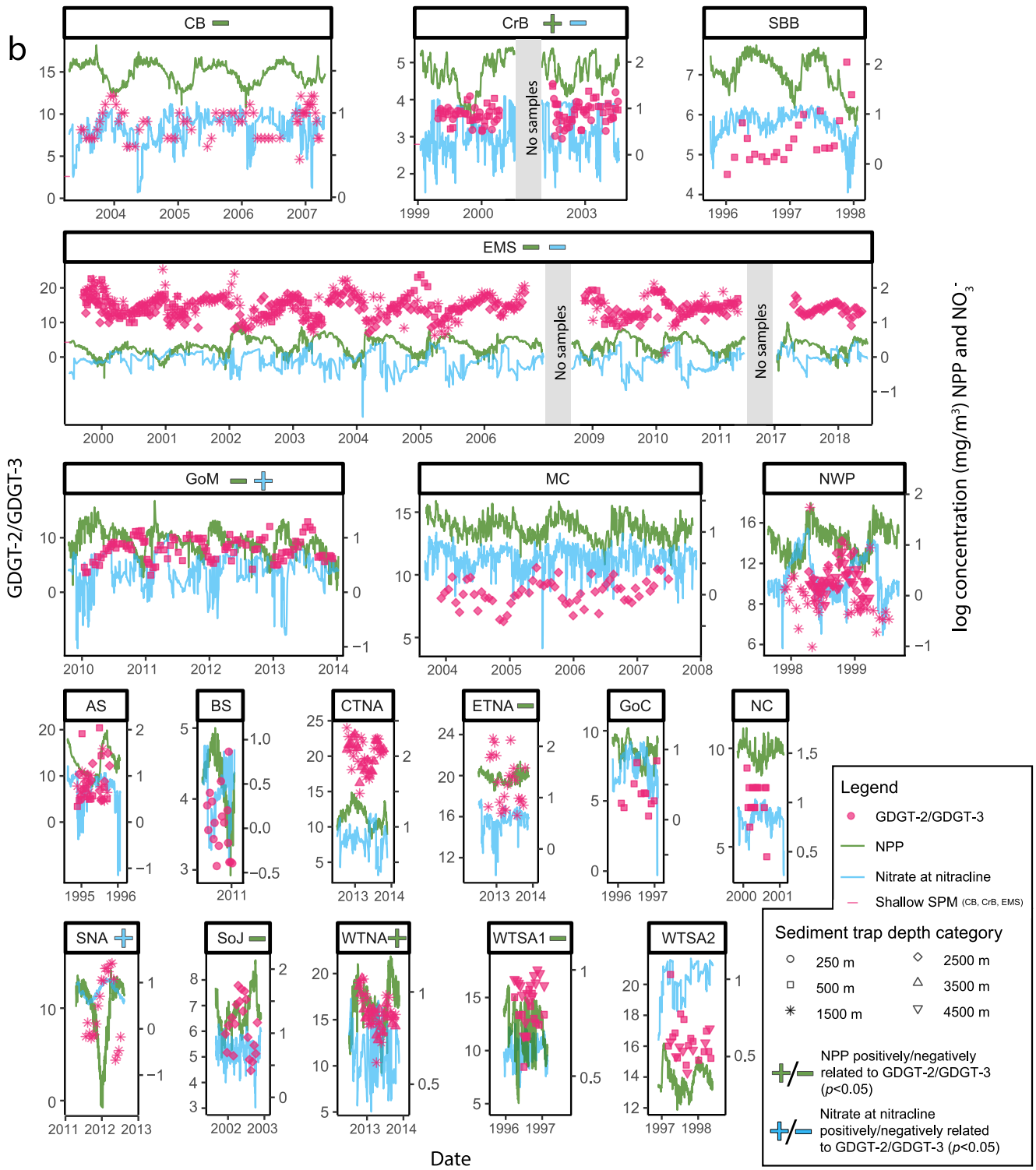

Figure 2. (Continued)

10.1029/2025PA005141

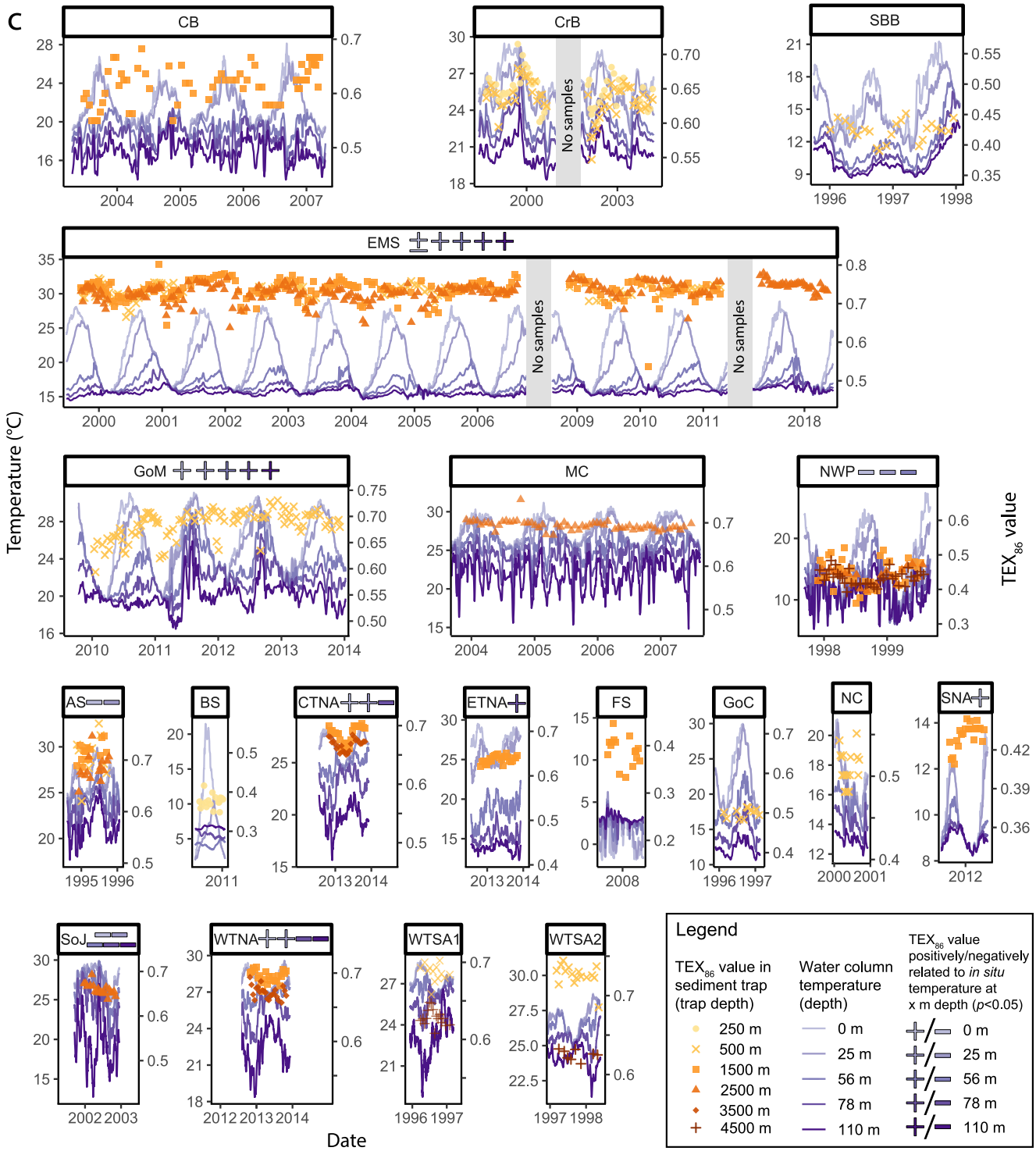

Figure 2. (Continued)

Significant correlations (95% confidence level; Figures 2a and 2b; Figure 3; Table S4 in Supporting Information S1) occur between GDGT-2/GDGT-3 and the nitracline depth (presumed depth of maximum GDGT production), the nitrate concentration at the nitracline, the depth of maximum NPP (presumed depth of particle packaging), and the quantity of NPP provided by the hindcast model. Both positive (4/16 sites total) and negative

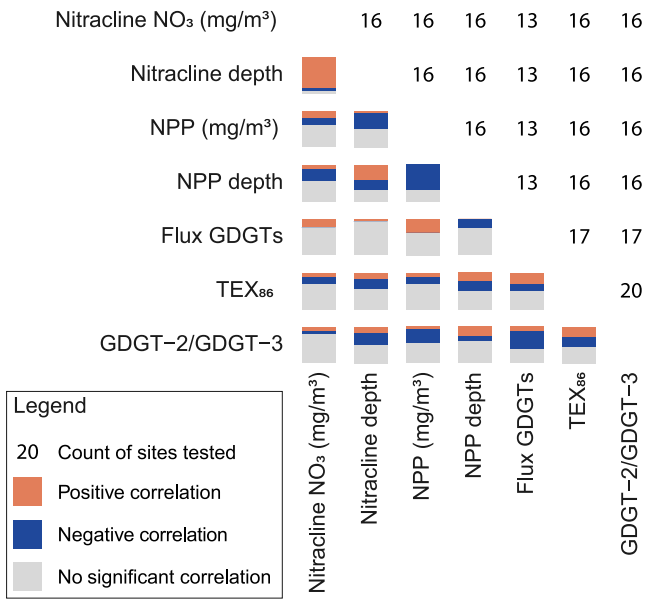

Figure 3. Pearson correlation results aggregated per site. Count of sites tested (excluding low GDGT-2/GDGT-3 sites) is shown in the upper right, and proportion of positive, negative, and no significant correlation ($p > 0.05$) shown in the bottom left.

(5/16 sites total) correlations are found between GDGT-2/GDGT-3 and the nitracline depth and/or nitrate concentration at the nitracline (Figure 3; Table S4 in Supporting Information S1). So, a shallower nitracline can lead to either lower or higher GDGT-2/GDGT-3 values, depending on the site. In addition, 3/13 sites have a positive correlation between GDGT flux and nitrate concentration at the nitracline (Figure 3; Table S4 in Supporting Information S1).

Increased/shallower maximum NPP is negatively correlated to GDGT-2/GDGT-3 at 7/16 sites (Figure 3; Table S4 in Supporting Information S1). This indicates that increased/shallower maximum NPP often leads to lower GDGT-2/GDGT-3 values. Furthermore, GDGT flux is correlated to increased and/or shallower maximum NPP at 6/13 sites (Figure 3; Table S4 in Supporting Information S1). Although the correlations between GDGT flux and increased and/or shallower maximum NPP are sometimes weak ($r = \pm 0.20$–0.92), their significance suggests that increased primary production leads to greater GDGT export.

Variations in TEX_{86} are often out of sync with upper 110 m water column temperatures (Figure 2c). Correlations between TEX_{86} and modeled in situ temperatures at 0, 25, 56, 78, and 110 m water depth can be positive or negative, depending on the site and water depth (range in r from −0.85 to 0.83; Figure 2c; Table S4 in Supporting Information S1). The presence of both positive and negative correlations indicates that seasonal changes in TEX_{86} values in sinking particles are not uniformly influenced by in situ temperatures.

The geographic and oceanographic setting (i.e., Atlantic vs. Pacific, upwelling vs. oligotrophic areas) and measurement of core versus total lipid GDGTs, do not exert any noticeable influence on whether a significant correlation occurs between sediment trap and model data in this study. Instead, the data-rich sites (7 multi-year records) are more likely to yield significant correlations.

4. Discussion

4.1. Contributions of Shallow Versus Deep Clade GDGTs in Sinking Particles Through Time and With Depth

Assuming that deep clade archaea produce GDGT-2/GDGT-3 in a ratio >5 (Rattanasriampaipong et al., 2022; Taylor et al., 2013), changes in GDGT-2/GDGT-3 values through time and with depth can indicate changes in the GDGT origin depth. The GDGT-2/GDGT-3 values in our data compilation suggest that sinking particles at nearly every sediment trap site globally contain GDGTs derived from the deep clade at some time of year (Figure 2ab; Figure S2 in Supporting Information S1). Seasonal or intra-annual changes in GDGT-2/GDGT-3 values observed in all but two sediment trap sites (Baltic Sea and Cariaco Basin; Figure 2ab) indicate temporal changes in GDGT origin depth at a given site. The overall agreement in GDGT-2/GDGT-3 values (<1.5 change; typically <0.05 for GDGT-2/(GDGT-2+GDGT-3) values) between trap depths at sites for which GDGT distributions from multiple depths are available (Table S5 in Supporting Information S1) indicates that there is little or no additional deep clade contributions from below the shallowest sediment trap (typically ~500 m), or that additional GDGT distributions are nearly identical to those captured in the shallowest sediment trap, confirming previous suggestions (Hurley et al., 2018; Schouten et al., 2002; Wuchter, Schouten, et al., 2006). Notably, at five sites, the flux of GDGTs increases below 500 m depth (Table S6 in Supporting Information S1), which could suggest that archaea contribute to the GDGT flux below 500 m. However, at these sites the total mass flux also increases below 500 m, or is similar between 500 and 4,500 m (Table S6 in Supporting Information S1), counter to expected and typical trends (i.e., Honjo et al., 2008). An increase in the total mass flux to the deeper sediment traps suggests that the deeper traps may be subject to sediment focusing (Siegel & Deuser, 1997) or receive resuspended sediments containing GDGTs (i.e., Mollenhauer et al., 2007), or that the upper sediment trap may have lower trapping efficiency than the deeper trap (i.e., Buesseler et al., 2007). Given the similar trends in GDGT and total mass fluxes through depth at these sites, we cannot conclude that GDGT export below 500 m contributes significantly to sedimentary GDGT distributions.

4.2. Linking Net Primary Production to the Origin Depth of GDGTs in Sinking Particles

We find a positive correlation between modeled NPP variables and GDGT flux to several sediment traps (Figure 3; Table S4 in Supporting Information S1). This is consistent with previous studies that found positive correlations between the fluxes of GDGTs and remains of primary producers in sediment traps (Chen et al., 2016; Mollenhauer et al., 2015; Park et al., 2018, 2019; Wuchter, Schouten, et al., 2006; Yamamoto et al., 2012) or with total mass flux (Huguet et al., 2007; Mollenhauer et al., 2015; Park et al., 2018; Rodrigo-Gámiz et al., 2015; Wuchter, Schouten, et al., 2006; Yamamoto et al., 2012). We also find that the depth of maximum NPP (positively) and amount of NPP (negatively) correlates to GDGT-2/GDGT-3 values (Figure 2ab; Figure 3; Table S4 in Supporting Information S1). This implies that NPP imposes controls on the origin depth of GDGTs in sinking particles on the studied time scales.

4.2.1. Correlations Between NPP and GDGT-2/GDGT-3

The amount of NPP and the depth of maximum NPP cannot be statistically distinguished in the present work, indicating that either or both could be the mechanism behind seasonal changes in GDGT-2/GDGT-3. Decreased/deeper maximum NPP implies deeper particle packaging, which could lead to increased incorporation of deep clade GDGTs and relatively higher GDGT-2/GDGT-3 values. However, the depth of maximum NPP is typically shallower than the presumed deep clade habitat of >100 m, while GDGT-2/GDGT-3 values >5 in all but three sediment traps indicate that these traps have received contributions of deep clade archaea (Figure 2a). Importantly, GDGT-2/GDGT-3 values that are >5 years-round at many sites suggest an input of deep clade GDGTs at all times of the year. This indicates that the GDGT export depth range extends into the deep clade habitat (>100 m), and is often deeper the depth of maximum NPP, year-round over much of the global ocean. It is thus possible that there is a continuous "background" export of GDGTs from the deeper clade, which is overprinted with shallow clade GDGTs by varying degrees.

4.2.2. GDGT-2/GDGT-3 as an NPP Proxy?

Because NPP variables and GDGT-2/GDGT-3 values are correlated at several sites, one might expect that GDGT-2/GDGT-3 could be applied as a proxy for NPP or the depth of maximum NPP. However, the relationship between the model depth of maximum NPP to GDGT-2/GDGT-3 cannot be directly, globally scaled. For example, GDGTs in sediment traps from Cape Blanc and the Gulf of Mexico have similar ranges in GDGT-2/GDGT-3, but the depth of maximum NPP is often much deeper in Gulf of Mexico (0–40 m vs. 0–100 m; Figure 2a). The different scaling per site is likely because GDGT distributions, and therefore GDGT-2/GDGT-3 values, are subject to several factors, such as temperature, pH, and the species/strains of GDGT producers (Bale et al., 2019; Elling et al., 2015; Rattanasriampaipong et al., 2022; Schouten et al., 2002). Seasonal and spatial differences in shallow clade GDGT production due to competition with Euryarchaeota and phytoplankton in the mixed layer (Lincoln et al., 2014; Wan et al., 2018) may also lead to differences in GDGT-2/GDGT-3 values. Furthermore, we have greatly simplified the complexities of the biological pump by using NPP as a descriptor of export processes. Export processes can be complicated by factors such as differences in mineral ballast between different groups of primary producers (Balch et al., 2010), ballasting due to dust deposition (Armstrong et al., 2001), and seasonality of the amount and depth of zooplankton fecal pelleting (Turner, 2002). Although each of these factors is related to NPP, they can impact NPP to varying degrees seasonally at a given site and between different sites. Variability in these aspects of the biological pump, which also lead to spatial variability in the data-model fit (E.U. Copernicus Marine Service Information (CMEMS), n.d.-a) could also lead to the mixed results found in this study. Future research into GDGT export could consider more sophisticated export models in which particle packaging below 100 m is quantified, rather than relying on NPP as an indicator of export.

Accordingly, the GDGT origin depth appears dynamic, and can vary by location and through seasonal and interannual changes in productivity and other controls on export depth. Although changes in the depth of maximum NPP can favor a shallower or deeper GDGT origin depth range, NPP is not the sole control on GDGT-2/GDGT-3 values when comparing sites. GDGT-2/GDGT-3 values may be useful as a qualitative proxy for GDGT origin depth at a given site. However, because the shallow clade endmember GDGT-2/GDGT-3 value is temperature-dependent (Rattanasriampaipong et al., 2022), independent estimates of productivity should be used when the proxy record indicates changes in temperature.

4.2.3. GDGT Sinking Rates

The correlations in this study were performed assuming that the response between NPP variables and GDGT-2/GDGT-3 occur with no or little time lag. This assumption suggests that increased maximum NPP leads to organic matter packaging and high sinking speeds. Rapid export is consistent with the association of core lipid GDGTs with larger particles in SPM (Ingalls et al., 2012), since larger particles generally sink more quickly (e.g., Alldredge & Silver, 1988). Correlation between increased/shallower maximum NPP and a higher flux of GDGTs (Table S4 in Supporting Information S1) further points to rapid sinking of GDGTs, since larger particles are more likely to form under higher-productivity conditions supported by high nutrient levels (Alldredge & Silver, 1988; Guidi et al., 2009; Turner, 2002).

However, GDGT incorporation into fast-sinking particles is at odds with the long lag time (80+ days) previously found to occur between TEX_{86} in sinking particles and instrumental SSTs at the Cape Blanc site (Mollenhauer et al., 2015), or satellite-based SSTs at Fram Strait and subpolar North Atlantic sites (Park et al., 2019; Rodrigo-Gámiz et al., 2015). Without lag, TEX_{86} values and upper ocean temperature are as likely to be positively as negatively correlated (Figure 2c). For a temperature control on seasonal variations in TEX_{86} values, having both positive and negative correlations would require that GDGTs sink at vastly different rates at different sites. Instead, the correlation between TEX_{86} and GDGT-2/GDGT-3 values at 11 out of 20 sites in our compilation suggests an ecological rather than thermal control on TEX_{86} values in sinking particles. If this is the case, the long lag times and slow sinking speeds calculated using TEX_{86} and upper ocean temperatures may be based on an erroneous assumption. So, rather than the slow sinking speeds and long lag time required to explain TEX_{86} variations in sinking particles at some sites, GDGTs are likely incorporated into relatively large, fast-sinking particles, and changes in GDGT distributions in sinking particles through the seasonal cycle are primarily related to seasonal changes in the GDGT origin depth at most studied sites. Direct testing with sinking velocity sediment traps (Wakeham et al., 2009) could better resolve the sinking speed of GDGT-containing particles.

Alternatively, long lag times between in situ temperatures and TEX_{86} response could also arise from a time lag between GDGT production and particle packaging, rather than lag due to sinking. In this scenario, archaeal cells may remain suspended in the water column for extended periods prior to export. We cannot exclude this scenario entirely, however, progressive degradation of older particles would remove them from the water column, likely favoring export of "fresh" GDGTs. Studies of intact polar lipids in sinking particles could yield further insight into GDGT packaging and export dynamics, and the timescale between GDGT production and export.

Nonetheless, export of GDGTs produced by deep clade archaea (GDGT-2/GDGT-3 > 5) occurs at some time of year on a near-global scale (Figure 2ab), albeit associated with lower GDGT flux (Table S4 in Supporting Information S1). The little export of GDGTs produced by deep clade archaea that does take place could possibly be regulated by their association with particles forming under lower-productivity conditions, which are often smaller and sink more slowly. These slow-sinking particles would allow more time for incorporation of GDGTs from deep archaea. Speculatively, coprophagy in deep waters may also incorporate deep clade GDGTs into sinking particles.

4.2.4. Nitracline Impact on GDGT-2/GDGT-3 Values

In contrast to NPP variables, a lack of consistent directionality in the correlation between GDGT-2/GDGT-3 and nitracline variables indicates that depth of maximum GDGT production (i.e., the nitracline) is not consistently correlated to the origin depth of GDGTs in sinking particles on seasonal time scales (Figure 2ab; Figure 3; Table S4 in Supporting Information S1). Instead, the apparent relationships may arise in part from correlation between nitracline variables and other environmental parameters, including NPP. Alternatively, nitracline variables may be locally important for the GDGT origin depth. Regardless, this finding suggests that approaches to understanding the GDGT origin depth in sediments from GDGT-2/GDGT-3 and GDGT concentrations in SPM, where maximum GDGT concentrations occur at and below the nitracline (e.g., Guo et al., 2024; Hernández-Sánchez et al., 2014; Hurley et al., 2018) may not be globally applicable.

4.3. Implications for Sedimentary GDGT Distributions

GDGT-2/GDGT-3 values >5 at some time of year in most sediment trap sites point to a near-global presence of deep clade GDGTs in sinking particles. However, lower GDGT-2/GDGT-3 values occur during periods of higher

GDGT flux, leading to a shallower flux-weighted GDGT origin depth. This is further reflected in surface sediments, where the GDGT-2/GDGT-3 values are similar to or lower (by up to 11 ratio values) than the flux-weighted average values in sediment traps at half of the locations for which sediments were analyzed (Table S5 in Supporting Information S1). Taken together, deep clade GDGTs are exported in most marine environments, but GDGT export mechanisms favor export of shallow clade GDGTs, in agreement with previous work (Shah et al., 2008), which is reflected in accumulated sediments.

Globally pervasive export of deep clade GDGTs is consistent with the widespread impact of deep clade GDGTs on GDGT distributions in global surface sediments, as indicated by high (>5) GDGT-2/GDGT-3 values in 360/611 surface sediments (van der Weijst et al., 2022). Although GDGT-2/GDGT-3 values in surface sediments correlate with water depth, there is large scatter in this relationship (Taylor et al., 2013). Variability in particle packaging processes between locations may help to explain this scatter, where some deep (>1000 m) surface sediments exhibit low (<5) GDGT-2/GDGT-3 values, and some shallow (<500 m) surface sediments have high GDGT-2/GDGT-3 values. Moreover, assuming that sedimentary GDGT-2/GDGT-3 values can be linked to the biological pump would imply that past global variability in the strength of the biological pump is profound, which may have implications for GDGT origin depth and TEX_{86} values archived in the sedimentary record.

Based on GDGT-2/GDGT-3 values, surface sediments have an overall shallower GDGT origin signal than suggested by flux-weighted values in sediment traps, indicating that either the sediment trap series do not adequately describe GDGT flux or that some post-depositional processes may impact GDGTs. Exceptional flux events not captured in the sediment trap series could favor export of shallow GDGTs, in line with organic carbon export processes which favor large flux events (Cael et al., 2021) such as those resulting from short-term bloom events. Lower GDGT-2/GDGT-3 values in sediments could also occur due to a preservation bias in which GDGTs in larger, faster-sinking, shallower origin particles or aggregates are less susceptible to post-depositional degradation.

In downcore records, increases in GDGT-2/GDGT-3 values could be indicative of deeper maximum NPP and/or a deeper nitracline. Both are typically linked to (thermal) stratification, where nutrient-depleted surface waters drive primary producers deeper into the water column (e.g., Richardson & Bendtsen, 2019), likely leading to greater incorporation of GDGTs from the deep clade into sinking particles. Notably, for GDGTs derived from shallow clade archaea, GDGT-2/GDGT-3 values decrease with increasing temperature, which is the expected thermal dependence of GDGT-2/GDGT-3 (Rattanasriampaipong et al., 2022). However, this is the opposite of what occurs in the global surface sediment data set (Taylor et al., 2013) and several downcore records (i.e., Auderset et al., 2019; Hou et al., 2023; van der Weijst et al., 2022), where higher values of GDGT-2/GDGT-3 are associated with higher TEX_{86} values. This indicates that warmer climates could lead to the export of a larger relative proportion of GDGTs from the deep clade. However, a recent compilation of GDGT data over the past 192 My indicates that contributions of deep clade GDGTs were suppressed during periods with greenhouse climate conditions prior to the Eocene-Oligocene Transition (Rattanasriampaipong et al., 2022). Thus, the complexity of the biological pump, in addition to other controls on GDGT-2/GDGT-3 values (including temperature), may obscure a relationship between GDGT-2/GDGT-3 values and stratified conditions in the paleo domain.

Stratification can also occur due to the presence of a shallow, nutrient-rich intermediate water mass, and is a possible cause of high GDGT-2/GDGT-3 values during late Miocene to Pleistocene cooling in the eastern equatorial Atlantic (van der Weijst et al., 2022) and during the Eocene-Oligocene transition (Rattanasriampaipong et al., 2022). A modern example of a location where oceanography exerts an influence on GDGT origin depth is the Mediterranean Sea. This basin is characterized by stratified conditions, where nutrient availability in surface waters is low year-round, and a shallow intermediate water mass is present at the base of the photic zone, leading to productivity in the lower photic zone near the permanent pycnocline and nitracline (Lavigne et al., 2015). Such conditions seem to be ideal for export of GDGTs from deep clade archaea, or disadvantageous for export of GDGTs from shallow clade archaea, resulting in a relatively lower contribution of GDGTs from shallow clade archaea than in most areas of the modern ocean (Besseling et al., 2019; Kim et al., 2015; Figure 2ab; Table S5 in Supporting Information S1). Consistently high (>12) GDGT-2/GDGT-3 values in tropical Atlantic sediment traps (CTNA, ETNA, WTNA, WTSA1, WTSA2; Figure 2ab; Table S5 in Supporting Information S1) suggest that low surface nutrient conditions prompt sub-mixed layer primary production also in other oligotrophic areas, leading to relatively more export of deep clade GDGTs. Indeed, the western tropical South Atlantic

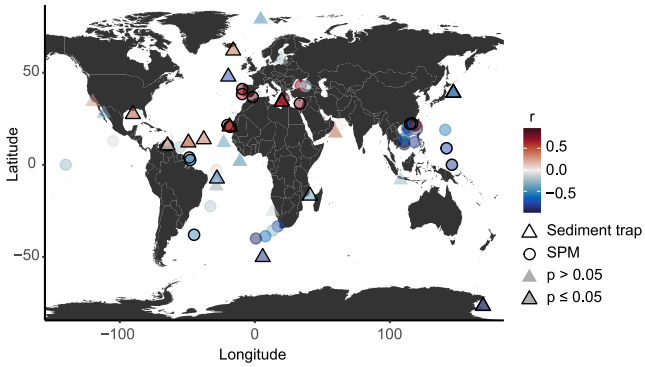

Figure 4. Map with sediment trap (triangle) and SPM (circle) locations, colored by the Pearson correlation coefficient (r) between GDGT-2/GDGT-3 and TEX_{86}. Locations with significant correlations ($p < 0.05$) are outlined in black.

sediment traps (WTSA1 and WTSA2) were moored in close proximity, but the higher GDGT-2/GDGT-3 values at WTSA2 imply less shallow clade-derived GDGTs (Figure 2ab; Table S5 in Supporting Information S1) because the NPP maximum at this location is lesser and deeper.

4.4. Ecological Impact on TEX_{86}

Because GDGT-2 and GDGT-3 are in both the numerator and denominator of TEX_{86}, changes in GDGT-2/GDGT-3 do not mathematically alter TEX_{86} values. Therefore, the impact of contributions from deep-dwelling archaea on GDGT-based temperature reconstructions has largely been thought to be minimal. This view has been further supported in studies of GDGTs in SPM depth profiles, which typically show little change in TEX_{86} values with depth compared to expected changes based on in situ temperatures (Basse et al., 2014; Hernández-Sánchez et al., 2014; Hurley et al., 2018; Turich et al., 2007; Wuchter et al., 2005). Limited differences in TEX_{86} were also found in two sediment core sets from coupled shallow-deep sites with correspondingly different GDGT-2/GDGT-3 ratios over the last 40 kyr (Varma et al., 2023). However, in this study we find significant correlations between TEX_{86} and GDGT-2/GDGT-3 in sinking particles at a given site (Figure 3; Table S4; Fig. S3 in Supporting Information S1), which indicate that mixing of shallow and deep clade GDGTs alters the seasonal TEX_{86} signal at many sites. Importantly, the correlation between TEX_{86} and GDGT-2/GDGT-3 can be either positive or negative, indicating that increased deep clade influence can either increase or decrease TEX_{86} values and derived temperatures.

To examine the spatial variability in the direction of the correlation between TEX_{86} and GDGT-2/GDGT-3, we use GDGTs in sediment trap material and suspended particulate matter (SPM), where SPM samples were grouped to have at least three data points within 150 km to check for correlation (Figure 4) (Basse et al., 2014; Besseling et al., 2019; Guo et al., 2024; Hernández-Sánchez et al., 2014; Hurley et al., 2018; Jia et al., 2017; Kim et al., 2015, p. 2016; Rattanasriampaipong et al., 2022; Schouten et al., 2012; Wakeham et al., 2004; Wei et al., 2011; Zell et al., 2014; Zhu et al., 2016). Although the spatial data coverage is still sparse, the North Atlantic Ocean and its subbasins (except for the Northeast Atlantic sediment trap), stand out with a positive correlation between GDGT-2/GDGT-3 and TEX_{86}, while GDGTs at all other sites have a negative or no (significant) correlation between these ratios. Because the correlations between TEX_{86} and GDGT-2/GDGT-3 have different directionality and magnitude of slopes depending on the location, the implications for paleothermometry cannot be globally generalized (Figure 4; Fig. S3 in Supporting Information S1). Notably, this spatial pattern differs from the spatial patterns of TEX_{86} residuals in the surface sediment data set used for the calibration of the proxy (Tierney & Tingley, 2014), which primarily shows latitudinal residual patterns. This indicates that the impact of deep clade GDGTs is not the controlling factor of the remaining spatially varying calibration uncertainty in the TEX_{86}.

4.5. Recommendations for Paleoclimate Studies

Traditionally, sedimentary GDGT-2/GDGT-3 values <5 are considered "low" and to have little influence from deep clade archaea (Taylor et al., 2013). As a result, paleoceanographic studies generally consider values near or below this value to primarily reflect a signal from shallow clade archaea, and thus that the temperature signal reflected by the GDGTs is reliable. However, GDGT-2/GDGT-3 values do not mix linearly. Therefore, we here use a mixing model to assess the influence of changing contributions of deep clade archaea to sedimentary ("mixed") GDGT-2/GDGT-3 values (Figure 5). For this model, we have used a deep clade endmember GDGT-2/GDGT-3 value of 50 based on reported GDGT-2/GDGT-3 values >50 or absence of GDGT-3 for SPM from the deep (>200 m) water column (Basse et al., 2014; Hernández-Sánchez et al., 2014; Hurley et al., 2018; Turich et al., 2013). Importantly, however, the mixing model is relatively insensitive to the deep clade endmember value (Fig. S4 in Supporting Information S1) due to the similarity of high GDGT-2/GDGT-3 values (25, 50, 100) when translated to the form of GDGT-2/(GDGT-2+GDGT-3) (~0.96, 0.98, 0.99, respectively) which decreases the sensitivity to low GDGT-3 abundances. In contrast, the model indicates that shallow clade endmember values have a large influence on the calculated relative contribution of deep clade archaea to the sediment. In general, shallow clade GDGT-2/GDGT-3 values decrease with increasing temperature (Rattanasriampaipong et al., 2022), in agreement with the principle that archaea generate relatively more rings under higher temperatures (Schouten

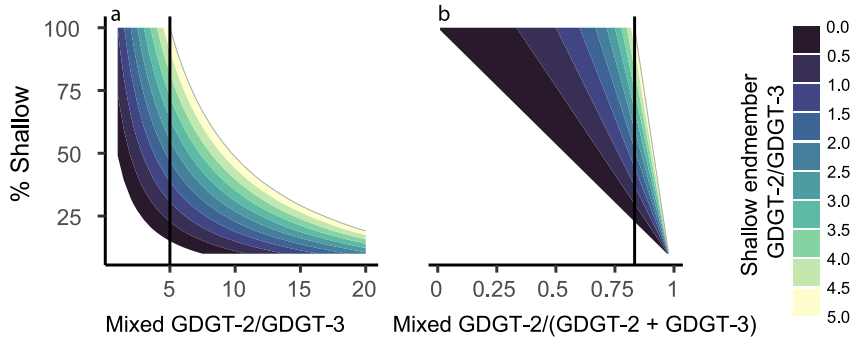

Figure 5. Theoretical shallow-deep mixing proportion of GDGT-2 and GDGT-3 for shallow endmember GDGT-2/GDGT-3 values from 0 to 5 and a deep endmember value of 50. The mixed (i.e., what would be measured in sediment) GDGT-2/GDGT-3 value (left) or GDGT-2/(GDGT-2+GDGT-3) value (right) is on *x* axis, and the proportion of the shallow endmember on the *y* axis. A mixed GDGT-2/GDGT-3 value of 5 as discussed in the text is highlighted for reference. The mixing model is relatively insensitive to the deep clade endmember value (see Fig. S4 in Supporting Information S1).

et al., 2002). As a result, a GDGT-2/GDGT-3 cutoff value of 5 could correspond to 100% shallow clade derived GDGTs in sediments from cold regions/climates where shallow clade archaea produce GDGT-2/GDGT-3 with value of 5, whereas in warm regions/climates a sedimentary GDGT-2/GDGT-3 value of 5 may represent deep clade GDGT contributions that make up >75% of the GDGT pool when shallow clade GDGT-2/GDGT-3 values are 0.5 (Figure 5). As a result, prior knowledge of the GDGT-2/GDGT-3 ratio produced by the shallow clade at a particular location would be necessary to begin to quantify mixing between the clades using this ratio. Since this information is not available during past climate states, this approach is unfortunately fruitless for paleoclimate studies, though full mixing models may become possible with future work defining how shallow clade GDGT distributions themselves vary with temperature.

Rather than using a cutoff value of 5, we suggest that future paleoceanographic studies assess the relationship between ecological and isoGDGT-based proxies to determine whether inputs from deep clade archaea systematically influence the reconstructed temperatures. Changes in TEX_{86} driven by varying relative contributions of deep clade GDGTs could bias downcore records to exhibit either more or less variability in temperature than occurred. Based on the correlations between GDGT-2/GDGT-3 and TEX_{86} in sediment traps, a hypothetical core at a location where no change in temperature occurred but with GDGT-2/GDGT-3 ratios varying from 4 to 10 could yield reconstructed temperatures that vary by up to 3°C purely due to shifts in the clade of GDGT producers. By extension, a larger change in reconstructed temperature (>0.5°C) per unit increase in GDGT-2/GDGT-3 likely indicates that factors aside from community composition (i.e., temperature or ammonia availability) contribute to changes in reconstructed temperature.

Investigating correlations between TEX_{86} and GDGT-2/GDGT-3 could therefore prove useful in disentangling temperature from ecologically driven changes in paleorecords. These correlations have previously been investigated in the Late Miocene to Pliocene part of the record from ODP site 959 in the eastern equatorial Atlantic (van der Weijst et al., 2022) and in the early Pliocene at DSDP site 609 in the northeastern Atlantic (Auderset et al., 2019), which are discussed here as examples. At ODP site 959, there is a positive correlation between GDGT-2/GDGT-3 and TEX_{86} with a slope of ∼7°C per unit increase in GDGT-2/GDGT-3 (van der Weijst et al., 2022). This slope is much larger than that observed in the currently studied sediment traps, where the maximum change in predicted temperature is ∼0.5°C per unit increase in GDGT-2/GDGT-3. The change in TEX_{86} at this site likely indicates a climate signal with relatively minor overprinting from deep clade archaea. By contrast, the positive correlation at DSDP site 609 in the northeastern Atlantic (Auderset et al., 2019) shows a change in TEX_{86}-derived temperatures of ∼0.5°C per unit increase in GDGT-2/GDGT-3 when including sediments with high (>14) GDGT-2/GDGT-3 values, in line with an ecological control on TEX_{86}. However, after excluding data with GDGT-2/GDGT-3 values > 14 from this downcore record these two parameters have little relationship. Furthermore, sediment layers with high GDGT-2/GDGT-3 values at DSDP site 609 have low mass accumulation rates of GDGTs and alkenones (Auderset et al., 2019), pointing to a weaker biological pump and little NPP, which could have led to relatively smaller contributions of shallow clade GDGTs with low GDGT-2/

GDGT-3 values (see 4.2.2). Productivity proxies may provide further insight into GDGT origin depth and are recommended to constrain downcore changes in the depth of GDGT temperature dependence.

Most importantly, we note the difference between GDGT origin depth and the depth of temperature dependence in sedimentary GDGTs. The GDGT origin depth range could include depths that are not inhabited by shallow clade archaea (>200 m). However, SPM profiles indicate that temperature-related changes in TEX_{86} values occur in the upper 100 m (Schouten et al., 2002; Sinninghe Damsté et al., 2002; Turich et al., 2007), where deep clade archaea are largely absent (Besseling et al., 2019; Villanueva et al., 2015). Although GDGTs with intact diglycosidic headgroups in SPM below 100 m depth exhibit a TEX_{86} temperature dependence for in situ temperatures <5°C, core lipid GDGTs below 100 m depth lack temperature dependence (Zhu et al., 2016). So, although the addition of deep clade GDGTs can overprint and alter the shallow-derived, thermally influenced TEX_{86} signal, the lack of TEX_{86} temperature dependence in deep clade GDGTs suggests that they do not contribute to the temperature dependence of TEX_{86} as stored in sediments. Rather than the deep clade GDGTs contributing to temperature dependence (i.e., resulting in lower TEX_{86}-derived temperatures due to a deeper, cooler habitat), we suggest that the shallow temperature-dependent GDGT pool is mixed with some deep clade endmember that has no effective thermal dependence for TEX_{86} thermometry. Therefore, rather than assuming a deep (>200 m) TEX_{86} temperature dependence, we recommend using temperature calibrations that do not extend deeper than the shallow clade habitat (0–200 m), and assessing how GDGT-2/GDGT-3 values may indicate deep clade overprinting.

In addition, quantification of GDGTs using an internal standard could aid in identifying periods of low biological pump activity when GDGT contributions from the shallow clade are relatively small. Low GDGT mass accumulation rates have sometimes been observed to occur with high GDGT-2/GDGT-3 values (Auderset et al., 2019; Hou et al., 2023). In a hypothetical marine environment with a constant low-level rain of deep clade GDGTs, sediments would have high GDGT-2/GDGT-3 values when surface export is minimal (Section 4.2.1). However, a stronger biological pump leads to relatively greater shallow clade GDGT export and higher GDGT concentrations, and mixing larger proportions of shallow clade GDGTs with low levels of deep clade GDGTs would lead to lower GDGT-2/GDGT-3 values.

5. Conclusions

We explored the drivers of seasonal variations in GDGT distributions in sinking particles in globally distributed marine sediment traps. Seasonal changes in TEX_{86} are generally small and often out of phase with changes in water column temperatures. Rather than related to temperature, seasonal variations in GDGT-2/GDGT-3 imply that GDGT distributions in settling particles are mostly controlled by seasonal changes in GDGT origin depth, where higher GDGT-2/GDGT-3 values indicate a smaller relative contribution from shallow clade archaea, or a larger relative contribution from deep clade archaea (e.g., Besseling et al., 2019). These changes are often related to the depth of maximum NPP or to the quantity of NPP, indicating that the strength of the biological pump controls the relative proportion of GDGTs exported from the shallow and deep clades. Mechanistically, a stronger biological pump, as indicated by increased/shallower maximum NPP, would lead to a relatively greater proportion of shallow clade GDGTs in sinking particles. This implies that the origin depth of sedimentary GDGTs is tightly coupled to export processes rather than to the depth of GDGT production. Combined with correlations to fluxes of primary producers and little difference in GDGT distributions between sediment traps set at different depths, this confirms that most GDGTs are exported from the upper water column (<500 m), and that GDGTs from the shallow clade (<200 m) are typically more abundant in time-averaged (i.e., over time scales relevant to the sedimentary record) sinking flux relative to the living stock of archaea in the water column. Large spatial variability in the modern biological pump (e.g., Honjo et al., 2008) may, therefore, contribute to spatial differences in modern GDGT origin depth; and analogously, changes in the biological pump through geologic time may lead to changes in GDGT origin depth in a given paleoceanographic record. Short (single-year) time series and the complexity of the biological pump, which is here simplified as NPP, may have led to the lack of correlation seen in several sediment trap sites, highlighting a need for long time series and export models that consider particle incorporation within the deep clade habitat (>100 m). Overall, these results support GDGT origin depths near and below the depth of maximum NPP, which can vary in depth from the mixed layer to 150 m depth, depending on the location, nutrient regime, and season. In addition, GDGT-2/GDGT-3 values consistently >5 years-round at some sites indicate that particle (re)packaging below 100 m is important for GDGT export.

Furthermore, changes in the contribution of GDGTs produced by shallow and deep clades are strongly correlated to changes in TEX_{86} and can alter TEX_{86}-based temperature reconstructions by up to ±0.5°C per unit increase in GDGT-2/GDGT-3. However, the directionality of this correlation is site-specific, where sites in the North Atlantic and its subbasins show a positive correlation between TEX_{86} and GDGT-2/GDGT-3, while other areas of the globe have the opposite correlation. Future paleoclimate studies should carefully assess the relationship between these ratios to consider whether changes in ecology may impact paleoclimate reconstructions, and consider using productivity proxies to better constrain changes in GDGT origin depth. Further work toward defining how GDGT distributions, rather than indices, vary with temperature could lead to mixing models to better quantify ecological mixing effects.

Conflict of Interest

The authors declare no conflicts of interest relevant to this study.

Data Availability Statement

Newly reported GDGT data from the EMS, RS, WTSA1, and WTSA2 are available at Pangaea (Rice et al., 2025). Compiled GDGT data from new and previously reported global sediment trap studies and corresponding surface sediments is included as a supplement to this publication (Table S3 in Supporting Information S1).

Acknowledgments
We thank K. Nierop, D. Eefting, M. Hoorweg, and J. Hefter for their assistance in the lab; NIOZ and technical team for mooring and recovery of sediment traps in Eastern Mediterranean, and P. van Santvoort and his team for sample splitting on board; B. van der Veen for analysis of Ross Sea samples; G. Fischer for deploying and recovering sediment traps at WTSA1 and WTSA2; Leonardo Langone, Lucilla Capotondi, and Mariangela Ravaioli for deploying and recovering the RS sediment trap and CNR-ISMAR Bologna is thanked for providing the Ross Sea sediment trap samples. This work was carried out under the program of the Netherlands Earth System Science Centre (NESSC), financially supported by the Netherlands Ministry of Education, Culture and Science (OCW). This project has received funding from the European Union's Horizon 2020 research and innovation program under the Marie Skłodowska-Curie, grant agreement No 847504 and from the Clusters of Excellence "The Ocean in the Earth System" at MARUM (Grant EXC309). A. Sluijs thanks the European Research Council for consolidator Grant 771497 (SPANC). We thank Dr. Rattanasriampaipong, Dr. Pancost, and Dr. Inglis for constructive feedback that improved our work.

References

Alldredge, A. L., & Silver, M. W. (1988). Characteristics, dynamics and significance of marine snow. *Progress in Oceanography*, *20*(1), 41–82. https://doi.org/10.1016/0079-6611(88)90053-5

Armstrong, R. A., Lee, C., Hedges, J. I., Honjo, S., & Wakeham, S. G. (2001). A new, mechanistic model for organic carbon fluxes in the ocean based on the quantitative association of POC with ballast minerals. *Deep Sea Research Part II: Topical Studies in Oceanography*, *49*(1), 219–236. https://doi.org/10.1016/S0967-0645(01)00101-1

Auderset, A., Martínez-García, A., Tiedemann, R., Hasenfratz, A. P., Eglinton, T. I., Schiebel, R., et al. (2019). Gulf stream intensification after the early Pliocene shoaling of the Central American Seaway. *Earth and Planetary Science Letters*, *520*, 268–278. https://doi.org/10.1016/j.epsl.2019.05.022

Balch, W. M., Bowler, B. C., Drapeau, D. T., Poulton, A. J., & Holligan, P. M. (2010). Biominerals and the vertical flux of particulate organic carbon from the surface ocean. *Geophysical Research Letters*, *37*(22). https://doi.org/10.1029/2010GL044640

Bale, N. J., Hennekam, R., Hopmans, E. C., Dorhout, D., Reichart, G. J., van der Meer, M., et al. (2019). Biomarker evidence for nitrogen-fixing cyanobacterial blooms in a brackish surface layer in the Nile River plume during sapropel deposition. *Geology*, *47*(11), 1088–1092. https://doi.org/10.1130/G46682.1

Basse, A., Zhu, C., Versteegh, G. J. M., Fischer, G., Hinrichs, K.-U., & Mollenhauer, G. (2014). Distribution of intact and core tetraether lipids in water column profiles of suspended particulate matter off Cape Blanc, NW Africa. *Organic Geochemistry*, *72*, 1–13. https://doi.org/10.1016/j.orggeochem.2014.04.007

Besseling, M. A., Hopmans, E. C., Koenen, M., van der Meer, M. T. J., Vreugdenhil, S., Schouten, S., et al. (2019). Depth-related differences in archaeal populations impact the isoprenoid tetraether lipid composition of the Mediterranean Sea water column. *Organic Geochemistry*, *135*, 16–31. https://doi.org/10.1016/j.orggeochem.2019.06.008

Bijl, P. K., Śliwińska, K. K., Duncan, B., Huguet, A., Naeher, S., Rattanasriampaipong, R., et al. (2025). Reviews and syntheses: Best practices for the application of marine GDGTs as proxy for paleotemperatures: Sampling, processing, analyses, interpretation, and archiving protocols. *Biogeosciences*, *22*(21), 6465–6508. https://doi.org/10.5194/bg-22-6465-2025

Buesseler, K. O., Antia, A., Chen, M., Fowler, S. W., Gardner, W. D., Gustafsson, O., et al. (2007). An assessment of the use of sediment traps for estimating upper ocean particle fluxes. *Journal of Marine Research*, *65*(3), 345–416. https://doi.org/10.1357/002224007781567621

Cael, B. B., Bisson, K., Conte, M., Duret, M. T., Follett, C. L., Henson, S. A., et al. (2021). Open Ocean particle flux variability from surface to seafloor. *Geophysical Research Letters*, *48*(9), 1–10. https://doi.org/10.1029/2021GL092895

Chen, W., Mohtadi, M., Schefuß, E., & Mollenhauer, G. (2016). Concentrations and abundance ratios of long-chain alkenones and glycerol dialkyl glycerol tetraethers in sinking particles south of Java. *Deep-Sea Research Part I Oceanographic Research Papers*, *112*, 14–24. https://doi.org/10.1016/j.dsr.2016.02.010

Close, H. G., Shah, S. R., Ingalls, A. E., Diefendorf, A. F., Brodie, E. L., Hansman, R. L., et al. (2013). Export of submicron particulate organic matter to mesopelagic depth in an oligotrophic gyre. *Proceedings of the National Academy of Sciences*, *110*(31), 12565–12570. https://doi.org/10.1073/pnas.1217514110

de Bar, M. W., Ullgren, J. E., Thunnell, R. C., Wakeham, S. G., Brummer, G.-J. A., Stuut, J.-B. W., et al. (2019). Long-chain diols in settling particles in tropical oceans: Insights into sources, seasonality and proxies. *Biogeosciences*, *16*(8), 1705–1727. https://doi.org/10.5194/bg-16-1705-2019

De Jonge, C., Peterse, F., Nierop, K. G. J., Blattmann, T. M., Alexandre, M., Ansanay-Alex, S., et al. (2024). Interlaboratory comparison of branched GDGT temperature and pH proxies using soils and lipid extracts. *Geochemistry, Geophysics, Geosystems*, *25*(7), e2024GC011583. https://doi.org/10.1029/2024GC011583

De Rosa, M., & Gambacorta, A. (1988). The lipids of archaebacteria. *Progress in Lipid Research*, *27*(3), 153–175. https://doi.org/10.1016/0163-7827(88)90011-2

Elling, F. J., Könneke, M., Mußmann, M., Greve, A., & Hinrichs, K. U. (2015). Influence of temperature, pH, and salinity on membrane lipid composition and TEX86 of marine planktonic thaumarchaeal isolates. *Geochimica et Cosmochimica Acta*, *171*, 238–255. https://doi.org/10.1016/j.gca.2015.09.004

E.U. Copernicus Marine Service Information (CMEMS). (n.d.-a). Global Ocean biogeochemistry Hindcast [Dataset]. *Marine Data Store (MDS)*. https://doi.org/10.48670/moi-00019

E.U. Copernicus Marine Service Information (CMEMS). (n.d.-b). Global Ocean physics reanalysis [Dataset]. *Marine Data Store (MDS)*. https://doi.org/10.48670/moi-00021

Fallet, U., Ullgren, J. E., Castañeda, I. S., van Aken, H. M., Schouten, S., Ridderinkhof, H., & Brummer, G. J. A. (2011). Contrasting variability in foraminiferal and organic paleotemperature proxies in sedimenting particles of the Mozambique Channel (SW Indian Ocean). *Geochimica et Cosmochimica Acta*, *75*(20), 5834–5848. https://doi.org/10.1016/j.gca.2011.08.009

Fokkema, C. D., Agterhuis, T., Gerritsma, D., de Goeij, M., Liu, X., de Regt, P., et al. (2023). Polar amplification of orbital-scale climate variability in the early Eocene greenhouse world. *Climate of the Past Discussions*, 1–26. https://doi.org/10.5194/cp-2023-70

Francis, C. A., Roberts, K. J., Beman, J. M., Santoro, A. E., & Oakley, B. B. (2005). Ubiquity and diversity of ammonia-oxidizing archaea in water columns and sediments of the ocean. *Proceedings of the National Academy of Sciences of the United States of America*, *102*(41), 14683–14688. https://doi.org/10.1073/pnas.0506625102

Guidi, L., Stemmann, L., Jackson, G. A., Ibanez, F., Claustre, H., Legendre, L., et al. (2009). Effects of phytoplankton community on production, size, and export of large aggregates: A world-ocean analysis. *Limnology & Oceanography*, *54*(6), 1951–1963. https://doi.org/10.4319/lo.2009.54.6.1951

Guo, J., Wang, Z., Achterberg, E. P., Yuan, H., Song, J., Wang, Y., et al. (2024). Variations in isoprenoid tetraether lipids through the water column of the Western Pacific Ocean: Implications for sedimentary TEX86 records. *Geochimica et Cosmochimica Acta*, *368*, 24–33. https://doi.org/10.1016/j.gca.2024.01.013

Hernández-Sánchez, M. T., Woodward, E. M. S., Taylor, K. W. R., Henderson, G. M., & Pancost, R. D. (2014). Variations in GDGT distributions through the water column in the South East Atlantic Ocean. *Geochimica et Cosmochimica Acta*, *132*, 337–348. https://doi.org/10.1016/j.gca.2014.02.009

Ho, S. L., & Laepple, T. (2016). Flat meridional temperature gradient in the early Eocene in the subsurface rather than surface ocean. *Nature Geoscience*, *9*(8), 606–610. https://doi.org/10.1038/ngeo2763

Honjo, S., Manganini, S. J., Krishfield, R. A., & Francois, R. (2008). Particulate organic carbon fluxes to the ocean interior and factors controlling the biological pump: A synthesis of global sediment trap programs since 1983. *Progress in Oceanography*, *76*(3), 217–285. https://doi.org/10.1016/j.pocean.2007.11.003

Hopmans, E. C., Schouten, S., & Sinninghe Damsté, J. S. (2016). The effect of improved chromatography on GDGT-based palaeoproxies. *Organic Geochemistry*, *93*, 1–6. https://doi.org/10.1016/j.orggeochem.2015.12.006

Hou, S., Lamprou, F., Hoem, F. S., Hadju, M. R. N., Sangiorgi, F., Peterse, F., & Bijl, P. K. (2023). Lipid-biomarker-based sea surface temperature record offshore Tasmania over the last 23 million years. *Climate of the Past*, *19*(4), 787–802. https://doi.org/10.5194/cp-19-787-2023

Huguet, C., Martens-Habbena, W., Urakawa, H., Stahl, D. A., & Ingalls, A. E. (2010). Comparison of extraction methods for quantitative analysis of core and intact polar glycerol dialkyl glycerol tetraethers (GDGTs) in environmental samples. *Limnology and Oceanography: Methods*, *8*(4), 127–145. https://doi.org/10.4319/lom.2010.8.127

Huguet, C., Schimmelmann, A., Thunell, R., Lourens, L. J., Damsté, J. S. S., & Schouten, S. (2007). A study of the TEX86 paleothermometer in the water column and sediments of the Santa Barbara Basin, California. *Paleoceanography*, *22*(3), 1–9. https://doi.org/10.1029/2006PA001310

Hurley, S. J., Lipp, J. S., Close, H. G., Hinrichs, K. U., & Pearson, A. (2018). Distribution and export of isoprenoid tetraether lipids in suspended particulate matter from the water column of the Western Atlantic Ocean. *Organic Geochemistry*, *116*, 90–102. https://doi.org/10.1016/j.orggeochem.2017.11.010

Ingalls, A. E., Huguet, C., & Truxal, L. T. (2012). Distribution of intact and core membrane lipids of archaeal glycerol Dialkyl glycerol tetraethers among size-fractionated particulate organic matter in hood canal, puget sound. *Applied and Environmental Microbiology*, *78*(5), 1480–1490. https://doi.org/10.1128/AEM.07016-11

Jia, G., Wang, X., Guo, W., & Dong, L. (2017). Seasonal distribution of archaeal lipids in surface water and its constraint on their sources and the TEX86 temperature proxy in sediments of the South China Sea. *Journal of Geophysical Research: Biogeosciences*, *122*(3), 592–606. https://doi.org/10.1002/2016JG003732

Karner, M. B., DeLong, E. F., & Karl, D. M. (2001). Archaeal dominance in the mesopelagic zone of the Pacific Ocean. *Nature*, *409*(6819), 507–510. https://doi.org/10.1038/35054051

Kim, J. H., Schouten, S., Hopmans, E. C., Donner, B., & Sinninghe Damsté, J. S. (2008). Global sediment core-top calibration of the TEX86 paleothermometer in the ocean. *Geochimica et Cosmochimica Acta*, *72*(4), 1154–1173. https://doi.org/10.1016/j.gca.2007.12.010

Kim, J. H., Schouten, S., Rodrigo-Gámiz, M., Rampen, S., Marino, G., Huguet, C., et al. (2015). Influence of deep-water derived isoprenoid tetraether lipids on the TEX^{H}_{86} paleothermometer in the Mediterranean Sea. *Geochimica et Cosmochimica Acta*, *150*, 125–141. https://doi.org/10.1016/j.gca.2014.11.017

Kim, J. H., van der Meer, J., Schouten, S., Helmke, P., Willmott, V., Sangiorgi, F., et al. (2010). New indices and calibrations derived from the distribution of crenarchaeal isoprenoid tetraether lipids: Implications for past sea surface temperature reconstructions. *Geochimica et Cosmochimica Acta*, *74*(16), 4639–4654. https://doi.org/10.1016/j.gca.2010.05.027

Könneke, M., Bernhard, A. E., de la Torre, J. R., Walker, C. B., Waterbury, J. B., & Stahl, D. A. (2005). Isolation of an autotrophic ammonia-oxidizing marine archaeon. *Nature*, *437*(7058), 543–546. https://doi.org/10.1038/nature03911

Lavigne, H., D'Ortenzio, F., Ribera D'Alcalà, M., Claustre, H., Sauzède, R., & Gacic, M. (2015). On the vertical distribution of the chlorophyll *a* concentration in the Mediterranean Sea: A basin-scale and seasonal approach. *Biogeosciences*, *12*(16), 5021–5039. https://doi.org/10.5194/bg-12-5021-2015

Lengger, S. K., Hopmans, E. C., Sinninghe Damsté, J. S., & Schouten, S. (2012). Comparison of extraction and work up techniques for analysis of core and intact polar tetraether lipids from sedimentary environments. *Organic Geochemistry*, *47*, 34–40. https://doi.org/10.1016/j.orggeochem.2012.02.009

Lincoln, S. A., Wai, B., Eppley, J. M., Church, M. J., Summons, R. E., & DeLong, E. F. (2014). Planktonic Euryarchaeota are a significant source of archaeal tetraether lipids in the ocean. *Proceedings of the National Academy of Sciences*, *111*(27), 9858–9863. https://doi.org/10.1073/pnas.1409439111

McClymont, E. L., Ganeshram, R. S., Pichevin, L. E., Talbot, H. M., van Dongen, B. E., Thunell, R. C., et al. (2012). Sea-surface temperature records of termination 1 in the Gulf of California: Challenges for seasonal and interannual analogues of tropical Pacific climate change. *Paleoceanography*, *27*(2). https://doi.org/10.1029/2011PA002226

Mollenhauer, G., Basse, A., Kim, J. H., Sinninghe Damsté, J. S., & Fischer, G. (2015). A four-year record of U^{K}_{37}'- and TEX^{H}_{86}-derived sea surface temperature estimates from sinking particles in the filamentous upwelling region off Cape Blanc, Mauritania. *Deep-Sea Research Part I Oceanographic Research Papers*, *97*, 67–79. https://doi.org/10.1016/j.dsr.2014.11.015

Mollenhauer, G., Inthorn, M., Vogt, T., Zabel, M., Sinninghe Damsté, J. S., & Eglinton, T. I. (2007). Aging of marine organic matter during cross-shelf lateral transport in the Benguela upwelling system revealed by compound-specific radiocarbon dating. *Geochemistry, Geophysics, Geosystems*, *8*(9). https://doi.org/10.1029/2007GC001603

Park, E., Hefter, J., Fischer, G., Hvitfeldt Iversen, M., Ramondenc, S., Nöthig, E. M., & Mollenhauer, G. (2019). Seasonality of archaeal lipid flux and GDGT-based thermometry in sinking particles of high-latitude oceans: Fram Strait (79°N) and Antarctic Polar Front (50°S). *Biogeosciences*, *16*(11), 2247–2268. https://doi.org/10.5194/bg-16-2247-2019

Park, E., Hefter, J., Fischer, G., & Mollenhauer, G. (2018). TEX86 in sinking particles in three eastern Atlantic upwelling regimes. *Organic Geochemistry*, *124*, 151–163. https://doi.org/10.1016/j.orggeochem.2018.07.015

Rattanasriampaipong, R., Zhang, Y. G., Pearson, A., Hedlund, B. P., & Zhang, S. (2022). Archaeal lipids trace ecology and evolution of marine ammonia-oxidizing archaea. *Proceedings of the National Academy of Sciences*, *119*(31), 1–10. https://doi.org/10.1073/pnas.2123193119

Rice, A., Park, E., Mollenhauer, G., Bouwmans, D., van Boxtel, A., De Lange, G. J., et al. (2025). Archaeal tetraether lipids in sinking particles in the Mediterranean Sea, Ross Sea, and western South Atlantic Ocean [dataset publication series] [Dataset]. *PANGAEA*. https://doi.org/10.1594/PANGAEA.983205

Richardson, K., & Bendtsen, J. (2019). Vertical distribution of phytoplankton and primary production in relation to nutricline depth in the open ocean. *Marine Ecology Progress Series*, *620*, 33–46. https://doi.org/10.3354/meps12960

Richardson, T. L. (2019). Mechanisms and pathways of small-phytoplankton export from the surface Ocean. *Annual Review of Marine Science*, *11*(1), 57–74. https://doi.org/10.1146/annurev-marine-121916-063627

Richardson, T. L., & Jackson, G. A. (2007). Small phytoplankton and carbon export from the surface Ocean. *Science*, *315*(5813), 838–840. https://doi.org/10.1126/science.1133471

Richey, J. N., & Tierney, J. E. (2016). GDGT and alkenone flux in the northern Gulf of Mexico: Implications for the TEX^{H}_{86} and U^{K}_{37}' paleothermometers. *Paleoceanography*, *31*(12), 1547–1561. https://doi.org/10.1002/2016PA003032

Rodrigo-Gámiz, M., Rampen, S. W., de Haas, H., Baas, M., Schouten, S., & Sinninghe Damsté, J. S. (2015). Constraints on the applicability of the organic temperature proxies $U^{K'}_{37}$, TEX_{86} and LDI in the subpolar region around Iceland. *Biogeosciences*, *12*(22), 6573–6590. https://doi.org/10.5194/bg-12-6573-2015

Schouten, S., Hopmans, E. C., Pancost, R. D., & Sinninghe Damsté, J. S. (2000). Widespread occurrence of structurally diverse tetraether membrane lipids: Evidence for the ubiquitous presence of low-temperature relatives of hyperthermophiles. *Proceedings of the National Academy of Sciences*, *97*(26), 14421–14426. https://doi.org/10.1073/pnas.97.26.14421

Schouten, S., Hopmans, E. C., Rosell-Melé, A., Pearson, A., Adam, P., Bauersachs, T., et al. (2013). An interlaboratory study of TEX86 and BIT analysis of sediments, extracts, and standard mixtures. *Geochemistry, Geophysics, Geosystems*, *14*(12), 5263–5285. https://doi.org/10.1002/2013GC004904

Schouten, S., Hopmans, E. C., Schefuß, E., & Sinninghe Damsté, J. S. (2002). Distributional variations in marine crenarchaeotal membrane lipids: A new tool for reconstructing ancient sea water temperatures? *Earth and Planetary Science Letters*, *204*(1–2), 265–274. https://doi.org/10.1016/S0012-821X(02)00979-2

Schouten, S., Huguet, C., Hopmans, E. C., Kienhuis, M. V. M., & Sinninghe Damsté, J. S. (2007). Analytical methodology for TEX86 paleothermometry by high-performance liquid chromatography/atmospheric pressure chemical ionization-mass spectrometry. *Analytical Chemistry*, *79*(7), 2940–2944. https://doi.org/10.1021/ac062339v

Schouten, S., Pitcher, A., Hopmans, E. C., Villanueva, L., van Bleijswijk, J., & Sinninghe Damsté, J. S. (2012). Intact polar and core glycerol dibiphytanyl glycerol tetraether lipids in the Arabian Sea oxygen minimum zone: I. Selective preservation and degradation in the water column and consequences for the TEX86. *Geochimica et Cosmochimica Acta*, *98*, 228–243. https://doi.org/10.1016/j.gca.2012.05.002

Shah, S. R., Mollenhauer, G., Ohkouchi, N., Eglinton, T. I., & Pearson, A. (2008). Origins of archaeal tetraether lipids in sediments: Insights from radiocarbon analysis. *Geochimica et Cosmochimica Acta*, *72*(18), 4577–4594. https://doi.org/10.1016/j.gca.2008.06.021

Siegel, D. A., & Deuser, W. G. (1997). Trajectories of sinking particles in the Sargasso Sea: Modeling of statistical funnels above deep-ocean sediment traps. *Deep Sea Research Part I: Oceanographic Research Papers*, *44*(9), 1519–1541. https://doi.org/10.1016/S0967-0637(97)00028-9

Sinninghe Damsté, J. S., Rijpstra, W. I. C., Hopmans, E. C., Prahl, F. G., Wakeham, S. G., & Schouten, S. (2002). Distribution of membrane lipids of planktonic crenarchaeota in the Arabian Sea. *Applied and Environmental Microbiology*, *68*(6), 2997–3002. https://doi.org/10.1128/AEM.68.6.2997-3002.2002

Taylor, K. W. R., Huber, M., Hollis, C. J., Hernandez-Sanchez, M. T., & Pancost, R. D. (2013). Re-evaluating modern and Palaeogene GDGT distributions: Implications for SST reconstructions. *Global and Planetary Change*, *108*, 158–174. https://doi.org/10.1016/j.gloplacha.2013.06.011

Tierney, J. E., & Tingley, M. P. (2014). A Bayesian, spatially-varying calibration model for the TEX_{86} proxy. *Geochimica et Cosmochimica Acta*, *127*, 83–106. https://doi.org/10.1016/j.gca.2013.11.026

Tierney, J. E., & Tingley, M. P. (2015). A TEX86 surface sediment database and extended Bayesian calibration. *Scientific Data*, *2*(1), 150029. https://doi.org/10.1038/sdata.2015.29

Turich, C., Freeman, K. H., Bruns, M. A., Conte, M., Jones, A. D., & Wakeham, S. G. (2007). Lipids of marine Archaea: Patterns and provenance in the water-column and sediments. *Geochimica et Cosmochimica Acta*, *71*(13), 3272–3291. https://doi.org/10.1016/j.gca.2007.04.013

Turich, C., Schouten, S., Thunell, R. C., Varela, R., Astor, Y., & Wakeham, S. G. (2013). Comparison of TEX86 and U37K' temperature proxies in sinking particles in the Cariaco Basin. *Deep-Sea Research Part I Oceanographic Research Papers*, *78*, 115–133. https://doi.org/10.1016/j.dsr.2013.02.008

Turner, J. T. (2002). Zooplankton fecal pellets, marine snow and sinking phytoplankton blooms. *Aquatic Microbial Ecology*, *27*(1), 57–102. https://doi.org/10.3354/ame027057

van der Weijst, C. M. H., van der Laan, K. J., Peterse, F., Reichart, G.-J., Sangiorgi, F., Schouten, S., et al. (2022). A 15-million-year surface- and subsurface-integrated TEX_{86} temperature record from the eastern equatorial Atlantic. *Climate of the Past*, *18*(8), 1947–1962. https://doi.org/10.5194/cp-18-1947-2022

Varma, D., Hättig, K., van der Meer, M. T. J., Reichart, G.-J., & Schouten, S. (2023). Constraining water depth influence on organic paleotemperature proxies using sedimentary archives. *Paleoceanography and Paleoclimatology*, *38*(6), e2022PA004533. https://doi.org/10.1029/2022PA004533

Villanueva, L., Schouten, S., & Sinninghe Damsté, J. S. (2015). Depth-related distribution of a key gene of the tetraether lipid biosynthetic pathway in marine Thaumarchaeota. *Environmental Microbiology*, *17*(10), 3527–3539. https://doi.org/10.1111/1462-2920.12508

Wakeham, S. G., Hopmans, E. C., Schouten, S., & Sinninghe Damsté, J. S. (2004). Archaeal lipids and anaerobic oxidation of methane in euxinic water columns: A comparative study of the Black Sea and Cariaco Basin. *Chemical Geology*, *205*(3–4), 427–442. https://doi.org/10.1016/j.chemgeo.2003.12.024

Wakeham, S. G., Lee, C., Peterson, M. L., Liu, Z., Szlozek, J., Putnam, I. F., & Xue, J. (2009). Organic biomarkers in the twilight zone—Time series and settling velocity sediment traps during MedFlux. *Deep-Sea Research Part II Topical Studies in Oceanography*, *56*(18), 1437–1453. https://doi.org/10.1016/j.dsr2.2008.11.030

Wan, X. S., Sheng, H.-X., Dai, M., Zhang, Y., Shi, D., Trull, T. W., et al. (2018). Ambient nitrate switches the ammonium consumption pathway in the euphotic ocean. *Nature Communications*, *9*(1), 915. https://doi.org/10.1038/s41467-018-03363-0

Wei, Y., Wang, J., Liu, J., Dong, L., Li, L., Wang, H., et al. (2011). Spatial variations in archaeal lipids of surface water and core-top sediments in the South China Sea and their implications for paleoclimate studies. *Applied and Environmental Microbiology*, *77*(21), 7479–7489. https://doi.org/10.1128/AEM.00580-11

Wittenborn, A. K., Radtke, H., Dutheil, C., Arz, H. W., & Kaiser, J. (2022). A downcore calibration of the TEX86L temperature proxy for the Baltic Sea. *Continental Shelf Research*, *251*, 104875. https://doi.org/10.1016/j.csr.2022.104875

Wuchter, C., Abbas, B., Coolen, M. J. L., Herfort, L., Van Bleijswijk, J., Timmers, P., et al. (2006). Archaeal nitrification in the ocean. *Proceedings of the National Academy of Sciences of the United States of America*, *103*(33), 12317–12322. https://doi.org/10.1073/pnas.0600756103

Wuchter, C., Schouten, S., Coolen, M. J. L., & Sinninghe Damsté, J. S. (2004). Temperature-dependent variation in the distribution of tetraether membrane lipids of marine Crenarchaeota: Implications for TEX86 paleothermometry. *Paleoceanography*, *19*(4). https://doi.org/10.1029/2004PA001041

Wuchter, C., Schouten, S., Wakeham, S. G., & Damsté, J. S. S. (2006). Archaeal tetraether membrane lipid fluxes in the northeastern Pacific and the Arabian Sea: Implications for TEX_{86} paleothermometry. *Paleoceanography*, *21*(4), 1–9. https://doi.org/10.1029/2006PA001279

Wuchter, C., Schouten, S., Wakeham, S. G., & Sinninghe Damsté, J. S. (2005). Temporal and spatial variation in tetraether membrane lipids of marine Crenarchaeota in particulate organic matter: Implications for TEX_{86} paleothermometry. *Paleoceanography*, *20*(3), 1–11. https://doi.org/10.1029/2004PA001110

Yamamoto, M., Shimamoto, A., Fukuhara, T., Tanaka, Y., & Ishizaka, J. (2012). Glycerol dialkyl glycerol tetraethers and TEX_{86} index in sinking particles in the western North Pacific. *Organic Geochemistry*, *53*, 52–62. https://doi.org/10.1016/j.orggeochem.2012.04.010

Zell, C., Kim, J.-H., Hollander, D., Lorenzoni, L., Baker, P., Silva, C. G., et al. (2014). Sources and distributions of branched and isoprenoid tetraether lipids on the Amazon shelf and fan: Implications for the use of GDGT-based proxies in marine sediments. *Geochimica et Cosmochimica Acta*, *139*, 293–312. https://doi.org/10.1016/j.gca.2014.04.038

Zhu, C., Wakeham, S. G., Elling, F. J., Basse, A., Mollenhauer, G., Versteegh, G. J. M., et al. (2016). Stratification of archaeal membrane lipids in the ocean and implications for adaptation and chemotaxonomy of planktonic archaea. *Environmental Microbiology*, *18*(12), 4324–4336. https://doi.org/10.1111/1462-2920.13289